Bragg scattering of nonlinear surface waves by sinusoidal sandbars

Haiqi Fang[1], Lian Tang[1]† and Pengzhi Lin[1]‡

[1]State Key Laboratory of Hydraulics and Mountain River Engineering, Sichuan University, Chengdu, 610065, China

(Received xx; revised xx; accepted xx)

Based on the multiple-scale expansion technique, a new set of extended nonlinear Schrödinger (ENLS) equations up to the third-order is derived to account for the additional effects of high-order bottom and dispersion effects, and nonlinear wave interaction on the wave transformation over periodic sandbars of sinusoidal geometry. By employing the small-amplitude wave assumption, a closed-form analytical solution for Bragg scattering is obtained from the linearized ENLS equations, which demonstrates that a downshift of the wave frequency of the maximum reflection is mainly due to the inclusion of high-order bottom effect. The factors that affect the downshift of the resonant frequency are identified and a theoretical expression in parabolic form is derived to quantify the downshift magnitude. The fully ENLS equations are solved numerically to further examine the influence of wave nonlinearity on the characteristics of Bragg resonance. The results reveal the existence of a critical water depth for a specific topography. When the water depth is larger than the critical value, the increase in wave nonlinearity will enhance the downshift magnitude of the Bragg resonance, while for water depth less than that value, the increase in wave nonlinearity will gradually change the Bragg resonance frequency from downshift to upshift.

Key words: Extended nonlinear Schrödinger equations, Bragg resonance, Downshift of the resonant frequency, Wave nonlinearity

---

MSC Codes *(Optional)* Please enter your MSC Codes here

1. Introduction

The Bragg resonance phenomenon, characterized by the partial reflection and transmission of incident waves over sinusoidal sandbars, exhibits the maximal reflection when the wavelength of the incident wave (λ) is approximately two times the wavelength of the sandbar undulations (λ_d). Initially confirmed in the laboratory by Davies and Heathershaw (1984), the phenomenon was further studied experimentally, particularly in relation to wave–current

† Email address for correspondence: tanglian@scu.edu.cn
‡ Email address for correspondence: cvelinpz@scu.edu.cn

interactions, by Magne et al. (2005) and Laffitte et al. (2021). The higher-order Bragg resonance under more complex resonance conditions has been investigated by Guazzelli et al. (1992) and Peng et al. (2019) through experimental measurements. The Bragg resonance phenomenon has usually been utilized to design artificial bars for coastal protection (Liu et al. 2015; Mei et al. 1988).

Wave scattering theories have been widely used to explain the Bragg resonance phenomenon. The full nonlinear potential flow theory, incorporating surface and bottom nonlinearity, is capable of accurately describing wave scattering. However, numerical approaches are required to solve the equations, as shown by Liu and Yue (1998) and Peng et al. (2019). To explore the analytical solutions or obtain simplified models, other water wave equations with different assumptions are employed. Starting from the surface-linearized Laplace equation, the analytical solutions including Floquet solutions (Howard and Yu 2007; Yu and Howard 2012) and perturbation solution (Davies and Heathershaw 1984) are derived. By further assuming the wavenumber varying with water depth, the surface-linearised Laplace equation can be simplified to the mild-slope-type equations, which are effective when the bottom amplitude and its variation are mild, leading to series form solutions as demonstrated by Liu et al. (2019), Liu and Zhou (2014), and Fang et al. (2023). Recently, Liang et al. (2020) combined mild slope equation with Mathieu Instability theory and derived a formula for phase downshift of Bragg resonance under the condition of infinite bottom length. Alternatively, the Boussinesq equation, as an integral model, can be used to describe weakly nonlinear wave propagation over varying topography in shallow water (Madsen et al. 2005; Gao et al. 2021), while usually numerical solution is the only viable access.

To derive the analytical solutions for wave scattering over varying topography, not restricted to shallow water condition, Mei (1985) developed wave envelope equations based on the multiple-scale expansion to analyse Bragg scattering by sandbars. The equations and solutions were subsequently extended to oblique incidence (Kirby 1993; Mei et al. 1988), doubly sinusoidal ripples (Rey et al. 1996), including the current effect (Ardhuin and Magne 2007; Fan et al. 2021; Kirby 1988), and random waves with an irregular bottom (Ardhuin and Herbers 2002). Furthermore, the approach of Mei (1985) was further extended to linear Schrödinger equations by Hara and Mei (1988) to include higher-order effects of bottom and dispersion to investigate wave-envelope evolution. Although their equations have difficulties to propose exact solutions for incident and reflected wave amplitudes due to the introduction of additional boundary conditions for continuity of pressure, their analysis demonstrated the importance of the higher-order effects of bottom and dispersion on Bragg scattering.

To include high-order effects induced by bottom, dispersion and the nonlinear wave interaction and to explore the underlying mechanisms of physical process of Bragg scattering, a new set of extended nonlinear Schrödinger (ENLS) equations is derived to describe wave scattering over periodic sinusoidal sandbars. This paper is organized as follows. In Section 2, the multiple-scale expansion method is utilised to formulate a system of nonlinear equations that considers high-order bottom and dispersion effects, as well as wave nonlinearity effect. In Section 3, analytical solutions for the reflection and transmission rates of the linearised equations are constructed, presenting an analysis of the generation of the wave components, and their mathematical expression in the equations after carefully considering the complex interactions. subsequently, the causes of the downshift behaviour are elucidated, and a theoretical formula for the downshift magnitude of the Bragg resonance is derived. In Section 4, a numerical approach to the full ENLS equations is implemented to further examine the influence of the wave nonlinearity on the Bragg resonance.

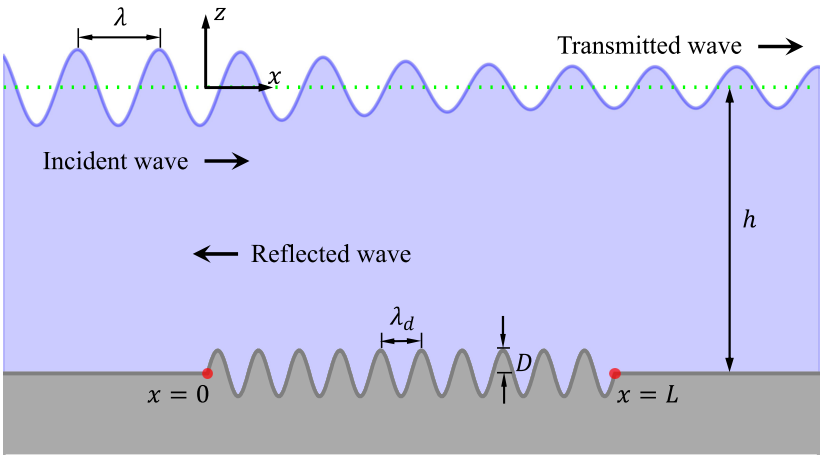

Figure 1: Schematic of wave propagation domain.

2. Mathematical derivation

2.1. *Derivation of the coupled model*

In this section, the extended nonlinear Schrödinger equations up to third-order are derived to consider the additional high-order bottom, dispersion effects and nonlinear wave interactions on wave transformation over spatially periodic cosine sandbars. As depicted in figure 1, waves propagate over cosine sandbars with an average water depth of h below the mean water surface, with D and k_d representing the amplitude and wavenumber of sandbars, respectively. The bottom wavelength $\lambda_d = 2\pi/k_d$ is the spacing between adjacent peaks from a cosine topography. In addition, waves are assumed to be periodic in both time and space, with ω and k denoting the wave frequency and wavenumber. The waves are allowed to slowly modulate in both time and space scale during the propagation process.

Assuming the weak nonlinearity of waves and topography, we give priority to the problems over $[0, L]$, where the associated parameters, namely, the wave amplitude of incident wave and amplitude of sinusoidal bars, are characterized by the same small parameter ε. Here, we denote ϕ as the velocity potential function, which satisfies the Laplace equation in the fluid domain,

$$\frac{\partial^2\phi}{\partial x^2} + \frac{\partial^2\phi}{\partial z^2} = 0 \quad (-h + \sigma < z < \eta), \tag{2.1}$$

where $\sigma = \sigma(x)$ and $\eta = \eta(x, t)$ are the bottom undulation above the mean bottom and free surface elevation, respectively. On the free surface, the kinematic and dynamic boundary conditions are:

$$\frac{\partial\eta}{\partial t} + \frac{\partial\phi}{\partial x}\frac{\partial\eta}{\partial x} - \frac{\partial\phi}{\partial z} = 0 \quad (z = \eta), \tag{2.2}$$

and

$$\frac{\partial\phi}{\partial t} + g\eta + \frac{1}{2}\left[\left(\frac{\partial\phi}{\partial x}\right)^2 + \left(\frac{\partial\phi}{\partial z}\right)^2\right] = 0 \quad (z = \eta). \tag{2.3}$$

Equations (2.2) and (2.3) are combined to give

$$\frac{\partial^2\phi}{\partial t^2} + g\frac{\partial\phi}{\partial z} + \frac{1}{2}\frac{\partial}{\partial t}\left[\left(\frac{\partial\phi}{\partial x}\right)^2 + \left(\frac{\partial\phi}{\partial z}\right)^2\right] - g\frac{\partial\phi}{\partial x}\frac{\partial\eta}{\partial x} = 0 \quad (z = \eta). \tag{2.4}$$

On the bottom, the no-flux boundary condition yields

$$\frac{\partial \phi}{\partial z} - \frac{\partial \phi}{\partial x}\frac{\partial \sigma}{\partial x} = 0 \quad (z = -h + \sigma). \tag{2.5}$$

To consider third-order effects on the Bragg resonance, the slow variables up to the second-order are introduced to capture the higher-order effects of sinusoidal bottom and wave–wave interactions.

$$\xi_1 = \varepsilon x, \quad \xi_2 = \varepsilon^2 x, \quad \tau_1 = \varepsilon t, \quad \tau_2 = \varepsilon^2 t. \tag{2.6}$$

The multiple-scale expansions for ϕ and η with third-order accuracy give:

$$\phi = \varepsilon^2 \phi_2 + \varepsilon^3 \phi_3 + \varepsilon \phi_1 + O(\varepsilon^4) \tag{2.7}$$

and

$$\eta = \varepsilon^2 \eta_2 + \varepsilon^3 \eta_3 + \varepsilon \eta_1 + O(\varepsilon^4). \tag{2.8}$$

in which $\phi_1 = \phi_1\left(x, z, t, \xi_1, \tau_1, \xi_2, \tau_2\right), \eta_1 = \eta_1\left(x, t, \xi_1, \tau_1, \xi_2, \tau_2\right)$, etc. $O(\ )$ is an infinitesimal of the same order. Notably, in comparison to the second-order analysis of Mei (1985), we utilize a third-order expansion and introduce two additional slow variables, ξ_2 and τ_2, to consider a third-order problem. Additionally, we take into account the nonlinear effect in the surface boundary condition, which is ignored by Mei (1985), accounting for wave-wave interactions and higher-order bottom and dispersion effects.

By substituting the solutions of (2.7) and (2.8) into (2.1) and utilizing the boundary conditions of (2.3), (2.4) and (2.5) with Taylor series expansions at $z = 0$ (for (2.3) and (2.4)) and $z = -h$ (for (2.5)), boundary value problems (BVPs) can be obtained for each order of ε upon separation of the different orders.

2.1.1. *The first-order problem*

The first-order problem is composed of waves propagating both forward and backwards, as Mei (1985) demonstrated, and an additional non-propagative mode, B, which was developed by Thomas et al. (2012). Assuming the associated potential and surface elevation can be expressed as

$$\phi_1 = \left(\psi^+ e^{iS^+} + \psi^- e^{iS^-} + C.C.\right) + B \tag{2.9}$$

and

$$\eta_1 = A^+ e^{iS^+} + A^- e^{iS^-} + C.C. \tag{2.10}$$

$C.C.$ denotes the conjugate component. The superscripts + and − refer to the incident and reflected waves, respectively. $\psi^\pm$ are the corresponding vertical profiles,

$$\psi^\pm = -\frac{gi}{2\omega}\frac{\cosh k(z+h)}{\cosh kh}A^\pm, \tag{2.11}$$

in which A^+ and A^- are the complex wave amplitudes, and B is a function, modulated by the slow variables,

$$A^\pm = A^\pm\left(\xi_1, \tau_1, \xi_2, \tau_2\right), \quad B^\pm = B^\pm\left(\xi_1, \tau_1, \xi_2, \tau_2\right). \tag{2.12}$$

S^+ and S^- are the phases,

$$S^\pm = \pm kx - \omega t \tag{2.13}$$

ω is the angular frequency and satisfies the dispersion equation, $\omega = gk \tanh kh$, while the wavenumber k should satisfy the standard Bragg resonance condition established by Mei (1985) to accurately capture wave reflection in the vicinity of the resonance,

$$k = \frac{k_d}{2}. \tag{2.14}$$

Thus, the cosine topography can be expressed in terms of the wavenumber k:

$$\sigma = \frac{D}{2}\left(e^{2ikx} + e^{-2ikx}\right). \tag{2.15}$$

2.1.2. *The Second-order problem*

At $O(\varepsilon^2)$, the BVP can be represented by the following system of equations

$$\frac{\partial^2\phi_2}{\partial x^2} + \frac{\partial^2\phi_2}{\partial z^2} = T_2 \quad (-h < z < 0), \tag{2.16}$$

$$\frac{\partial^2\phi_2}{\partial t^2} + g\frac{\partial\phi_2}{\partial z} = P_2 \quad (z = 0), \tag{2.17}$$

$$\frac{\partial\phi_2}{\partial z} = Q_2 \quad (z = -h), \tag{2.18}$$

$$\eta_2 = R_2 \quad (z = 0). \tag{2.19}$$

where T_2, P_2, Q_2 and R_2 are compulsory components consisting of lower-order terms. Let $S^+_{m,n}$ and $S^-_{m,n}$ denote the phase functions for waves propagating in the forward and backward directions, expressed as:

$$S^{\pm}_{m,n} = \pm mkx - n\omega t, \tag{2.20}$$

in particular, $S^{\pm} = S^{\pm}_{1,1}$. Moreover, it is assumed that ϕ_2 is represented as a series of multiple harmonics

$$\phi_2 = \gamma^{2,+}_{0,0} + \sum_{\substack{mn=0\\ m+n>0}}\left(\gamma^{2,+}_{m,n}e^{iS^+_{m,n}} + \text{C. C.}\right) + \sum_{m=1}^{\infty}\sum_{n=0}^{\infty}\left(\gamma^{2,+}_{m,n}e^{iS^+_{m,n}} + \gamma^{2,-}_{m,n}e^{iS^-_{m,n}} + \text{C. C.}\right). \tag{2.21}$$

The functions $\gamma^{2,\pm}_{m,n} = \gamma^{2,\pm}_{m,n}(z, \xi_1, \tau_1, \xi_2, \tau_2)$ corresponding to $e^{iS^{\pm}_{m,n}}$ for the second-order problem can be solved from equations (2.16) - (2.18) (detailed in Appendix 6.1), and ϕ_2 can be expressed as

$$\begin{aligned}\phi_2 = {} & \gamma^{2,+}_{1,1}e^{iS^+_{1,1}} + \gamma^{2,-}_{1,1}e^{iS^-_{1,1}} + \gamma^{2,+}_{2,2}e^{iS^+_{2,2}} + \gamma^{2,-}_{2,2}e^{iS^-_{2,2}} \\ & + \gamma^{2,+}_{0,2}e^{iS^+_{0,2}} + \gamma^{2,+}_{3,1}e^{iS^+_{3,1}} + \gamma^{2,-}_{3,1}e^{iS^-_{3,1}} + C.C.,\end{aligned} \tag{2.22}$$

in which the expressions of $\gamma^{2,+}_{1,1}$, etc., can be found in Appendix 6.2. Then, from (2.19), η_2 can be derived,

$$\begin{aligned}\eta_2 = {} & \beta^{2,+}_{0,0} + \left(\beta^{2,+}_{2,0}e^{iS^+_{2,0}} + \beta^{2,+}_{1,1}e^{iS^+_{1,1}} + \beta^{2,-}_{1,1}e^{iS^-_{1,1}} + \beta^{2,+}_{2,2}e^{iS^+_{2,2}}\right. \\ & \left. + \beta^{2,-}_{2,2}e^{iS^-_{2,2}} + \beta^{2,+}_{3,1}e^{iS^+_{3,1}} + \beta^{2,-}_{3,1}e^{iS^-_{3,1}} + C.C.\right).\end{aligned} \tag{2.23}$$

As demonstrated in Appendix 6.1, the following solvable conditions must be satisfied to ensure the solutions for $\gamma^{2,\pm}_{1,1}e^{iS^{\pm}_{1,1}}$

$$\frac{\partial A^{\pm}}{\partial\tau_1} + C^{\pm}_g\frac{\partial A^{\pm}}{\partial\xi_1} + iD^{\pm}_0A^{\mp} = 0. \tag{2.24}$$

in which $C^{\pm}_g$ and $D^{\pm}_0$ are the group velocities and topography-induced terms, respectively. (2.24) is equivalent to the envelope equations established by Mei (1985).

2.1.3. *The third-order problem*

For the third-order problem, the solvable conditions of the singular modes, $e^{iS^{+}_{1,1}}$ and $e^{iS^{-}_{1,1}}$, and the zero mode $e^{iS^{+}_{0,0}}$ are considered in the present solution. The other harmonics in the compulsory terms, which have no association with resonance, are not considered here. Consequently, all compulsory terms can be unified into a single expression:

$$\theta_3 = \theta^{3,+}_{0,0} + \left(\theta^{3,+}_{1,1} e^{iS^{+}} + \theta^{3,-}_{1,1} e^{iS^{-}} + C.C.\right) + O.T., \tag{2.25}$$

in which θ represents the forcing items T, P and Q, and $O.T.$ denotes other terms. $\theta^{3,+}_{0,0}$, $\theta^{3,+}_{1,1}$ and $\theta^{3,-}_{1,1}$ can be derived by substituting lower-order solutions, ϕ_2, η_2, ϕ_1 and η_1 to the differential form expressions of θ_3, shown in Appendix 6.2.

At the order of ε^3, (6.24) yields solvability conditions for singular components, $e^{iS^{\pm}_{1,1}}$, by way of the Green Formula depicted in (6.23)

$$\int_{-h}^{0} T^{3,\pm}_{1,1} \psi^{\pm} dz = \frac{1}{g} P^{3,\pm}_{1,1} \left.\psi^{\pm}\right|_{z=0} - Q^{3,\pm}_{1,1} \left.\psi^{\pm}\right|_{z=-h}, \tag{2.26}$$

which can be further integrated with the substitution of $T^{3,\pm}_{1,1}$, etc., resulting in two coupled equations for A^{+}, A^{-} and B

$$\begin{aligned} &\frac{\partial A^{\pm}}{\partial \tau_2} + C^{\pm}_g \frac{\partial A^{\pm}}{\partial \xi_2} + B^{\pm}_1 \frac{\partial^2 A^{\pm}}{\partial \tau_1^2} + B^{\pm}_2 \frac{\partial^2 A^{\pm}}{\partial \xi_1 \partial \tau_1} + B^{\pm}_3 \frac{\partial^2 A^{\pm}}{\partial \xi_1^2} + D^{\pm}_1 \frac{\partial A^{\mp}}{\partial \tau_1} + D^{\pm}_2 \frac{\partial A^{\mp}}{\partial \xi_1} \\ &+ D^{\pm}_3 A^{\pm} + \left\{\sigma^{\pm}_1 \left|A^{\pm}\right|^2 + \sigma^{\pm}_2 \left|A^{\mp}\right|^2 + \sigma^{\pm}_3 \frac{\partial B}{\partial \tau_1} + \sigma^{\pm}_4 \frac{\partial B}{\partial \xi_1}\right\} A^{\pm} = 0, \end{aligned} \tag{2.27}$$

in which $|A^{\pm}|$ corresponds the modulus of $A^{\pm}$, given by $\sqrt{A^{\pm}\left(A^{\pm}\right)^{*}}$.

It can be demonstrated that the zero mode of $T^{3,+}_{0,0}$ is not contingent upon z. Thus, the Laplace equation and bottom boundary condition supply a general solution for $\gamma^{3,\pm}_{0,0}$, with C_0 being an arbitrary complex

$$\gamma^{3,\pm}_{0,0} = \frac{1}{2} T^{3,+}_{0,0} z^2 + \left(Q^{3,+}_{0,0} + h T^{3,+}_{0,0}\right) z + C_0. \tag{2.28}$$

A solvability condition for B is derived to satisfy the surface boundary condition

$$g\left(h T^{3,+}_{0,0} + Q^{3,+}_{0,0}\right) = P^{3,+}_{0,0}. \tag{2.29}$$

By introducing the expressions of $T^{3,+}_{0,0}$, etc., (2.29) is transformed into a hyperbolic partial differential equation

$$\frac{\partial^2 B}{\partial \tau_1^2} - gh \frac{\partial^2 B}{\partial \xi_1^2} = \frac{\omega^4 - g^2 k^2}{4\omega^2} \frac{\partial\left(|A^{+}|^2 + |A^{-}|^2\right)}{\partial \tau_1} + \frac{g^2 k}{2\omega} \frac{\partial\left(|A^{+}|^2 - |A^{-}|^2\right)}{\partial \xi_1}. \tag{2.30}$$

We multiply (2.24) by $\left(A^{\pm}\right)^{*}$ and, upon conjugation and summation, obtain

$$\frac{\partial\left(|A^{+}|^2 + |A^{-}|^2\right)}{\partial \tau_1} + C^{+}_g \frac{\partial\left(|A^{+}|^2 - |A^{-}|^2\right)}{\partial \xi_1} = 0, \tag{2.31}$$

which indicates that (2.30) can be automatically satisfied by constructing the formulation of

$$\frac{\partial B}{\partial \tau_1} = -C_g^+ \lambda \left(\left|A^+\right|^2 + \left|A^-\right|^2 \right), \quad \frac{\partial B}{\partial \xi_1} = \lambda \left(\left|A^+\right|^2 - \left|A^-\right|^2 \right), \tag{2.32}$$

in which

$$\lambda = \frac{1}{C_g^{+2} - gh} \left(\frac{g^2 k}{2\omega} - C_g^+ \frac{\omega^4 - g^2 k}{4\omega^2} \right). \tag{2.33}$$

By introducing the first-order derivatives of B from (2.32) into (2.27), we can eliminate the terms related to it and thereby attain the second set of solvability conditions for $A^\pm$

$$\begin{aligned} &\frac{\partial A^\pm}{\partial \tau_2} + C_g^\pm \frac{\partial A^\pm}{\partial \xi_2} + B_1^\pm \frac{\partial^2 A^\pm}{\partial \tau_1^2} + B_2^\pm \frac{\partial^2 A^\pm}{\partial \xi_1 \partial \tau_1} + B_3^\pm \frac{\partial^2 A^\pm}{\partial \xi_1^2} + D_1^\pm \frac{\partial A^\mp}{\partial \tau_1} \\ &+ D_2^\pm \frac{\partial A^\mp}{\partial \xi_1} + D_3^\pm A^\pm + \left\{ F_1^\pm \left|A^\pm\right|^2 + F_2^\pm \left|A^\mp\right|^2 \right\} A^\pm = 0. \end{aligned} \tag{2.34}$$

Equation (2.34) can be reduced to the linear Schrödinger equation derived by Hara and Mei (1988), if wave-wave interaction is neglected and the transformations to (2.24) are implemented. However, their equation formulates a partial differential equation with respect to the second-order derivative of the spatial variable x, necessitating additional boundary conditions for continuity of pressure, thereby posing a challenge for seeking exact solutions. Therefore, they derived the ratio of the envelope height at antinodes in the strip to the envelope height at the strip's edge to settle for the second best. In the present study, to directly identify the solutions for incident and reflected wave evolutions, the differential transformations on (2.24) are employed to replace the second derivatives with respect to x in (2.34) as follows

$$\begin{aligned} \frac{\partial^2 A^\pm}{\partial \xi_1^2} &\to -\frac{iD_0^\pm}{C_g^\pm} \frac{\partial A^\mp}{\partial \xi_1} - \frac{1}{C_g^\pm} \frac{\partial^2 A^\pm}{\partial \tau_1 \partial \xi_1}, \\ \frac{\partial^2 A^\pm}{\partial \tau_1 \partial \xi_1} &\to -\frac{iD_0^\pm}{C_g^\pm} \frac{\partial A^\mp}{\partial \tau_1} - \frac{1}{C_g^\pm} \frac{\partial^2 A^\pm}{\partial \tau_1^2}. \end{aligned} \tag{2.35}$$

And we introduce transforms of temporal and spatial scales to recover x and t

$$\varepsilon \frac{\partial}{\partial \tau_1} + \varepsilon^2 \frac{\partial}{\partial \tau_2} \to \frac{\partial}{\partial t}, \quad \varepsilon \frac{\partial}{\partial \xi_1} + \varepsilon^2 \frac{\partial}{\partial \xi_2} \to \frac{\partial}{\partial x}, \tag{2.36}$$

which enables $A^\pm(\xi_1, \tau_1, \xi_2, \tau_2)$ to return to $A^\pm(x,t)$ and thus obtain a set of coupled nonlinear equations for $A^+$and A^-, and can be employed to investigate the envelope evolution of waves:

$$\begin{aligned} &\frac{\partial A^+}{\partial t} + C_g^+ \frac{\partial A^+}{\partial x} + iD_0^+ A^- + \overbrace{\left(D_1^+ - \frac{iB_2^+ D_0^+}{C_g^+} + \frac{iB_3^+ D_0^+}{\left(C_g^+\right)^2} \right) \frac{\partial A^-}{\partial t} + \left(D_2^+ - \frac{iB_3^+ D_0^+}{C_g^+} \right) \frac{\partial A^-}{\partial x} + D_3^+ A^+}^{\text{high-order bottom effect}} \\ &+ \underbrace{\left(B_1^+ - \frac{B_2^+}{C_g^+} + \frac{B_3^+}{\left(C_g^+\right)^2} \right) \frac{\partial^2 A^+}{\partial t^2}}_{\text{high-order dispersion effect}} + \underbrace{F_1^+ \left|A^+\right|^2 A^+ + F_2^+ \left|A^-\right|^2 A^+}_{\text{nonlinear wave interaction}} = 0, \end{aligned} \tag{2.37}$$

$$\frac{\partial A^-}{\partial t}+C_g^-\frac{\partial A^-}{\partial x}+iD_0^-A^+\overbrace{+\left(D_1^--\frac{iB_2^-D_0^-}{C_g^-}+\frac{iB_3^-D_0^-}{\left(C_g^-\right)^2}\right)\frac{\partial A^+}{\partial t}+\left(D_2^--\frac{iB_3^-D_0^-}{C_g^-}\right)\frac{\partial A^+}{\partial x}+D_3^-A^-}^{\text{high-order bottom effect}}$$
$$+\underbrace{\left(B_1^--\frac{B_2^-}{C_g^-}+\frac{B_3^-}{\left(C_g^-\right)^2}\right)\frac{\partial^2A^-}{\partial t^2}}_{\text{high-order dispersion effect}}+\underbrace{F_1^-\left|A^-\right|^2A^-+F_2^-\left|A^+\right|^2A^-}_{\text{nonlinear wave interaction}}=0. \tag{2.38}$$

Equations (2.37) and (2.38) are the newly derived ENLS equations, consisting of the basic governing equations of Mei (1985) (the first three items), the bottom effect terms with $D_0^\pm$ represents the first-order bottom effect and $D_1^\pm, D_2^\pm$ and $D_3^\pm$ are second-order bottom effects, the high-order wave dispersion effect terms ($B_1^\pm$, etc.) and the wave-wave interaction terms with $F_1^\pm$ and $F_2^\pm$ related to the nonlinear effect of wave-wave interactions. All detailed expressions can be found in Appendix 6.2.

Although the derivation of (2.37) and (2.38) is based on a cosine type of topography, they are applicable for sinusoidal sandbars through a translational transformation of x, if necessary. In addition, the newly derived equations can be applied to horizontal bottoms by eliminating topography-related terms without loss of generality.

The internal correlations between the newly derived ENLS and the previous versions of the NLS are summarized: If the topography related terms are eliminated and the substitution of $\partial^2/\partial t^2$ for $\partial^2/\partial x\partial t$ and $\partial^2/\partial x^2$ is applied in accordance with the first solvable conditions, as prescribed by (2.24), the ENLS is reduced to a range of variants of the NLS. Moreover, if the water depth is assumed to be infinite and the wave components that are affected by the varying bottom and reflection are excluded, the ENLS can be seen to be analogous to the CNLS equations established by Onorato et al. (2006), despite some minor discrepancies. Furthermore, the ENLS is accurately degenerated to the NLS equation of Liao et al. (2017) if the influence of the current is neglected.

3. Exact solution for the linearised ENLS equations

3.1. *Derivation of the exact solution*

Closed-form solutions for the ENLS equations are difficult to propose due to the nonlinearity derived from the wave-wave interactions. However, by assuming wave amplitudes to be sufficiently small, the equations can be reduced to a linear system coupling A^+ and A^-, leading to exact solutions, which enables systematic investigation on the influence of topographical factors on Bragg resonance. Therefore, in this section, by neglecting the wave nonlinearity, the linearised ENLS equations are obtained

$$\frac{\partial A^+}{\partial t}+C_g^+\frac{\partial A^+}{\partial x}+iD_0^+A^-+\left(B_1^+-\frac{B_2^+}{C_g^+}+\frac{B_3^+}{\left(C_g^+\right)^2}\right)\frac{\partial^2A^+}{\partial t^2}+\left(D_1^+-\frac{iB_2^+D_0^+}{C_g^+}+\frac{iB_3^+D_0^+}{\left(C_g^+\right)^2}\right)\frac{\partial A^-}{\partial t}$$
$$+\left(D_2^+-\frac{iB_3^+D_0^+}{C_g^+}\right)\frac{\partial A^-}{\partial x}+D_3^+A^+=0, \tag{3.1}$$

$$\frac{\partial A^-}{\partial t} + C_g^- \frac{\partial A^-}{\partial x} + iD_0^- A^+ + \left(B_1^- - \frac{B_2^-}{C_g^-} + \frac{B_3^-}{(C_g^-)^2} \right) \frac{\partial^2 A^-}{\partial t^2} + \left(D_1^- - \frac{iB_2^- D_0^-}{C_g^-} + \frac{iB_3^- D_0^-}{(C_g^-)^2} \right) \frac{\partial A^+}{\partial t} + \left(D_2^- - \frac{iB_3^- D_0^-}{C_g^-} \right) \frac{\partial A^+}{\partial x} + D_3^- A^- = 0. \tag{3.2}$$

As illustrated in figure 1, an incident wave train of both temporally and spatially periodic arrives from $x = -\infty$ and these waves are continuously reflected by the bottom sandbars, forming reflected waves that propagate in the reverse direction and produce standing waves by the superposition of the incident and reflected waves. In the region $x > L$, where the varying topography vanishes, only the forward propagating mode exists, designated as transmitted waves. The region $0 < x < L$ is highlighted by periodic sinusoidal bars of amplitude D and wavenumber $2k$, and L is the total length of the sandbars and $N_d = L/\lambda_d$ denotes the number of sandbars.

Let the incident and reflected waves be slightly detuned from the Bragg resonance, with their wave frequencies being $\omega^+ = \omega^- = \omega + \omega'$, where ω' implies wavenumber deviations k' and k'' for the incident and reflected waves, respectively. Over the sandbars $0 < x < L$, we can find solutions like

$$A^+ = A_0 T(x) e^{ik'x - i\omega' t} \quad (0 < x < L) \tag{3.3}$$

and

$$A^- = A_0 R(x) e^{-ik''x - i\omega' t} \quad (0 < x < L). \tag{3.4}$$

On the left side of the sandbars, we have

$$A^+ = A_0 e^{ik'x - i\omega' t} \quad (x < 0) \tag{3.5}$$

and

$$A^- = A_0 R(0) e^{-ik''x - i\omega' t} \quad (x < 0) \tag{3.6}$$

Note that the wavenumbers of the incident and reflected wave are

$$k^+ = k + k', \quad k^- = k + k''. \tag{3.7}$$

These wavenumbers can be substituted into (3.1) and (3.2) with topography-terms vanishing to obtain

$$k' = -\frac{iB_1^+ (\omega')^2 - \omega'}{S_4^+}, \quad k'' = -\frac{iB_1^- (\omega')^2 - \omega'}{S_4^-}. \tag{3.8}$$

The dispersion relation can be derived from (3.8), yielding

$$k^+ = k^- = k - \frac{iB_1^+ (\omega')^2 - \omega'}{S_4^+} \tag{3.9}$$

On the side $x > L$, only transmission occurs, indicating that

$$A^+ = A_0 T(L) e^{ik'x - i\omega' t} \quad (x > L) \tag{3.10}$$

and

$$A^- = 0 \quad (x > L) \tag{3.11}$$

Let $\tilde{R}$ and $\widetilde{T}$ denote the reflection and transmission rates, given by $|R(0)|$ and $|T(L)|$. The governing equations (3.1) and (3.2) can be expressed in terms of $T(x)$ and $R(x)$. $\tilde{()}$ represents

the first-order differential operator on x, and the equations can be expressed as

$$\begin{aligned} S_1^+ R(x) + S_2^+ T(x) + S_3^+ \dot{R}(x) + S_4^+ \dot{T}(x) = 0 \\ S_1^- T(x) + S_2^- R(x) + S_3^- \dot{T}(x) + S_4^- \dot{R}(x) = 0, \end{aligned} \tag{3.12}$$

where

$$\begin{aligned} S_1^+ = S_1^- = E_1 \omega' + i D_0^+ \\ S_2^+ = S_2^- = -i\omega' + E_2 \left(\omega'\right)^2 + D_3^+ \\ S_3^+ = -S_3^- = E_3 \\ S_4^+ = -S_4^- = C_g^+ \end{aligned} \tag{3.13}$$

in which E_1, E_2 and E_3 are coefficients, expressed as

$$\begin{aligned} E_1 = -i D_1^+ + \frac{D_0^+ \left(B_3^+ - B_2^+ C_g^+\right)}{\left(C_g^+\right)^2} \\ E_2 = -B_1^+ + \frac{-B_3^+ + B_2^+ C_g^+}{\left(C_g^+\right)^2} \\ E_3 = D_2^+ - \frac{-i B_3^+ D_0^+}{C_g^+}. \end{aligned} \tag{3.14}$$

The boundary conditions for $T(x)$ and $R(x)$ are given by

$$R(L) = 0, \quad T(0) = 1 \tag{3.15}$$

The linear equations (3.12) with the associated boundary conditions outlined by (3.15) constitute a solvable BVP, yielding an exact solution for the reflection rate, $\tilde{R}$. More details can be found in Appendix 6.3

$$\tilde{R} = \sqrt{\frac{Q_1^2}{|P \cot PL|^2 + Q_2^2}}, \tag{3.16}$$

in which Q_1, Q_2 and P are functions of ω' :

$$\begin{aligned} Q_1 = Q_1\left(\omega'\right) = \frac{-i\left\{E_3\left[D_3^+ + \omega'\left(-i + E_2\omega'\right)\right] + C_g^+\left(E_1\omega' + iD_0^+\right)\right\}}{E_3^2 - \left(C_g^+\right)^2} \\ Q_2 = Q_2\left(\omega'\right) = \frac{E_3 D_0^+ - i\left\{E_1 E_3 \omega' + C_g^+\left[D_3^+ + \omega'\left(-i + E_2\omega'\right)\right]\right\}}{E_3^2 - \left(C_g^+\right)^2} \\ P = P\left(\omega'\right) = \sqrt{\frac{\left(D_3^+ + \omega'\left(-i + E_2\omega'\right)\right)^2 - \left(E_1\omega' + iD_0^+\right)^2}{E_3^2 - \left(C_g^+\right)^2}}. \end{aligned} \tag{3.17}$$

It is evident that the only difference between the present solution (3.16) and the solution of Mei (1985) lies in the terms Q_1, Q_2 and P. If the higher-order contributions of E_1, E_2, E_3 and D_3^+ are set to zero, the present solution reduces to Mei's (1985) solution

$$\tilde{R}_{\mathrm{M}} = \sqrt{\frac{Q_{1,\mathrm{M}}^2}{Q_{2,\mathrm{M}}^2 + |P_{\mathrm{M}} \cot P_{\mathrm{M}} L|^2}}, \tag{3.18}$$

Case	h(m)	D/h	k_d(/m)	λ_d(m)	N_d	L(m)
D1	0.312	0.160	2π	1.0	10	10
L1	0.220	0.159	4π	0.5	10	5

Table 1: Parameters for wave scattering by sinusoidal sandbars.

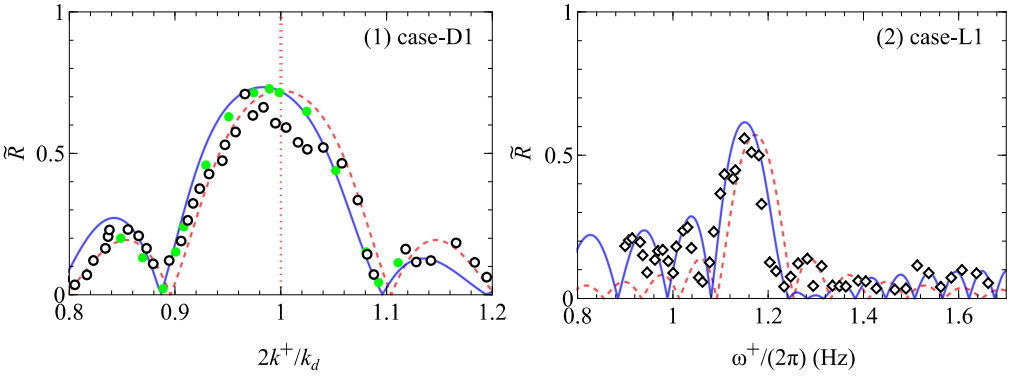

Figure 2: Comparison of the reflection rate $\tilde{R}$ for case-D1 and case-L1 among the present solution in (3.16) (blue solid line), analytical solution from Mei (1985) in (3.18) (red dashed line), numerical solutions of Liu and Yue (1998) (green dots) and experimental data from Davies and Heathershaw (1984) (black circles) and Laffitte et al. (2021) (black diamond), respectively. (1) case D1; (2) case L1.

in which

$$Q_{1,\mathrm{M}} = Q_{1,\mathrm{M}}(\omega') = \frac{D_0^+}{C_g^+}$$
$$Q_{2,\mathrm{M}} = Q_{2,\mathrm{M}}(\omega') = \frac{\omega'}{C_g^+} \tag{3.19}$$
$$P_{\mathrm{M}} = P_{\mathrm{M}}(\omega') = \sqrt{\frac{(\omega')^2 - \left(D_0^+\right)^2}{\left(C_g^+\right)^2}},$$

where the subscript M represents the solution of Mei (1985). $Q_{1,\mathrm{M}}, Q_{2,\mathrm{M}}$ and P_{M} are even functions with respect to ω', indicating good symmetry with $\tilde{R}_{\mathrm{M}}(\omega') = \tilde{R}_{\mathrm{M}}(-\omega')$ and the maximum reflection occurring at $\omega' = 0$. However, as evidenced by the inequalities of $Q_1(\omega') \neq Q_1(-\omega')$, $Q_2(\omega') \neq Q_2(-\omega')$ and $P(\omega') \neq P(-\omega')$, the present solution is not symmetrically distributed, which could potentially shift the positions of maximum reflection.

3.2. *Verifications of the solution for reflection*

To verify the analytical solution for reflection in (3.16), experiment-based wave scattering by sinusoidal sandbars is investigated. The geometrical configuration of the experimental setup is depicted in figure 1. The performance of the present solution is verified by comparing it with the experiments conducted by Davies and Heathershaw (1984) and Laffitte et al. (2021), denoted as D1 and L1, respectively. The wave- and topographic-related parameters of the experiments are shown in table 1.

Variables	The present solution	Liu and Yue (1998)	Madsen et al. (2005)	Liang et al. (2020)	Mei (1985)
$2k^+/k_d$	0.984	0.989	0.980	0.991	1
$\tilde{R}$	0.724	0.728	0.718	0.731	0.719

Table 2: The wavenumber and the reflection rate of the peak Bragg resonance.

Figure 2 shows the comparisons of the reflection $\tilde{R}$ obtained from the present solution, the analytical solution from Mei (1985), the numerical solution of Liu and Yue (1998), and the measured data by Davies and Heathershaw (1984) and Laffitte et al. (2021). The red dotted lines in figure 2 (1) signify $2k^+/k_d = 1$, which is the peak of the Bragg resonance predicted by Mei (1985). However, in practice, a slight phase downshift is commonly observed, as indicated by the numerical solutions of Liu and Yue (1998) and the measured data, which is accurately captured by the present solution. In prior research studies, the downshift characteristics for case D1 were investigated (Liang et al. 2020; Madsen et al. 2005), and the results of these studies are summarized in table 2.

Table 2 presents the results of the wavenumber and reflection for case D1 by the present solution, numerical solutions from Liu and Yue (1998), Madsen et al. (2005) and Liang et al. (2020). As can be observed, the wavenumber of the Bragg resonance is well predicted by the present analytical solution, while Mei's (1985) theory fails in this regard, highlighting the ability of the present solution to describe the downshift behaviour of Bragg resonance.

While the phenomenon of the downshift of the wave frequency upon resonance has been extensively reported, providing essential parameters for the design of artificial bars for coastal protection, the underlying mechanism for its formation remains elusive. Therefore, it is of great significance to elucidate the mechanism of the downshift behaviour and explore the influencing factors on the magnitude of the downshift of the wave frequency based on the present solutions.

3.3. *Frequency downshift of the Bragg resonance*

3.3.1. *Derivation of the downshift magnitude*

In this section, we first present a theoretical expression of the downshift magnitude of the wave frequency. The solution of reflection rate, denoted as $\tilde{R} = \tilde{R}(\omega')$, is expressed in (3.16). The wave frequency shift at maximum reflection, denoted as δ, can be obtained from the derivative of the reflection rate with respect to ω' being equal to zero:

$$\frac{d}{d\omega'}\left(\tilde{R}(\omega')\right)^2\Big|_{\omega'=\delta} = 0, \tag{3.20}$$

Employing the Taylor expansion of ω' and D to approximate the solution,

$$\begin{aligned}\delta &\approx \delta_0 + \delta_2 \\ &= \frac{3iC_g^+\left(E_3 + iE_1C_g^+\right)}{6E_2E_3C_g^+ - iL^2D_0^+} + \frac{\eth_4L^4 + \eth_2L^2}{5C_g^+\left(6E_2E_3C_g^+ - iL^2D_0^+\right)^2}\end{aligned} \tag{3.21}$$

This is detailed in Appendix 6.4. In Mei's (1985) theory, the coefficients E_1, E_2, E_3 and $D_3^\pm$ are excluded, implying that $\eth_4 = \eth_2 = 0$ (the definitions of $\eth_4$ and $\eth_2$ can refer to equations

Case	Variables	The Present solution	$D_1^+=0$	$D_2^+=0$	$D_3^+=0$	$B_1^+=0$	$B_2^+=0$	$B_3^+=0$
D1	$2k^+/k_d$	0.984	0.992	0.987	0.990	0.983	0.980	0.984
L1	$\omega^+/2\pi$	1.118	1.146	1.135	1.124	1.121	1.117	1.118

Table 3: The influence of B_s^+ and D_s^+ on the wavenumber or the wave frequency of the Bragg resonance.

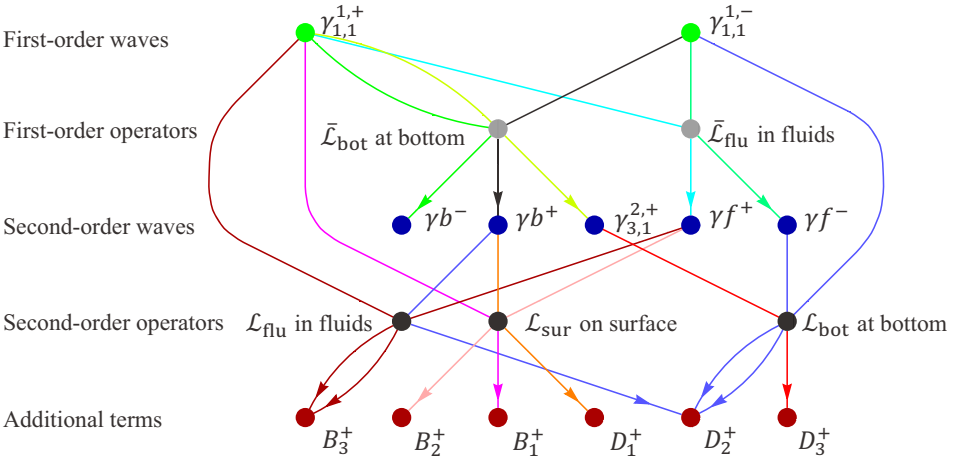

Figure 3: Illustration of the correlations between the wave components and the additional terms (red points).

(6.52) and (6.53)). This causes the parameters δ_0 and δ_2 to equal 0. Thus, $\delta = 0$ indicates a zero wave frequency shift.

3.3.2. *Formation of the downshift behaviour*

Compared to the governing equations in Mei (1985), the additional terms, i.e., $B_s^\pm$ and $D_s^\pm$ (s = 1, 2, 3) in the present solutions are proven to be the cause of downshift behaviour. The following work is to identify the most influential term with respect to the wavenumber or wave frequency in the cases of D1 and L1 by setting each term to zero one by one, of which the terms related to the superscript + are considered.

Table 3 presents the impact of B_s^+ and D_s^+ $(s = 1, 2, 3)$ on the wavenumber or wave frequency of the Bragg resonance. The downshift behaviour is impacted by each of the terms, with D_1^+ holding primacy over the two cases. The bottom-induced terms, D_s^+, are more influential than the dispersion-related items, B_s^+. To further explore the significance of these terms, their generation process in the present equations is investigated.

Figure 3 demonstrates the correlations among the terms of the equations, operators and wave components. The generation of these elements is elicited by three second-order differential operators for potential functions, defined in fluids ($\mathcal{L}_{\text{flu}}$), on the surface ($\mathcal{L}_{\text{sur}}$) and at the bottom ($\mathcal{L}_{\text{bot}}$), as well as first-order operators $\left(\overline{\mathcal{L}}_{\text{flu}} \text{ and } \overline{\mathcal{L}}_{\text{bot}}\right)$, the details of which are provided in Appendix 6.2. Seven wave components in the potential function contribute to B_s^+ and D_s^+, comprising second-order modes, namely, the non-resonant element $\gamma_{3,1}^{2,+}e^{iS_{3,1}^+}$ and resonant elements $\gamma b^\pm e^{iS_{1,1}^\pm}$ and $\gamma f^\pm e^{iS_{1,1}^\pm}$, as well as first-order resonant modes, i.e.,

$\gamma_{1,1}^{1,\pm}e^{iS_{1,1}^{\pm}}$. The second-order modes are induced by $\gamma_{1,1}^{1,\pm}e^{iS_{1,1}^{\pm}}$ through the first-order operators $\overline{\mathcal{L}}_{\text{flu}}$ and $\overline{\mathcal{L}}_{\text{bot}}$, and the non-resonant mode $\gamma_{3,1}^{2,+}e^{iS_{3,1}^{+}}$ is expressed as

$$\gamma_{3,1}^{2,+}=\frac{3igDk^2\operatorname{sech}kh\left(3gk\cosh 3kz+\omega^2\sinh 3kz\right)}{4\omega\left(3k\omega^2\cosh 3kh-9gk^2\sinh 3kh\right)}A^{+} \tag{3.22}$$

which is generated by $\gamma_{1,1}^{1,+}e^{iS_{1,1}^{+}}\xrightarrow{\overline{\mathcal{L}}_{\text{bot}}}\gamma_{3,1}^{2,+}e^{iS_{3,1}^{+}}$. The resonant modes include four components, given by

$$\gamma_{1,1}^{2,\pm}e^{iS_{1,1}^{\pm}}=\gamma b^{\pm}e^{iS_{1,1}^{\pm}}+\gamma f^{\pm}e^{iS_{1,1}^{\pm}} \tag{3.23}$$

in which $\gamma_{1,1}^{2,\pm}e^{iS_{1,1}^{\pm}}$is composed of bottom-forced component $\left(\gamma b^{\pm}e^{iS_{1,1}^{\pm}}\right)$and fluid-modulated component $\left(\gamma f^{\pm}e^{iS_{1,1}^{\pm}}\right)$.

$$\gamma b^{\pm}=-\frac{ikDg\sinh k(z+h)}{4\omega\cosh kh}A^{\mp} \tag{3.24}$$

and

$$\gamma f^{\pm}=\mp\frac{g(z+h)\sinh k(z+h)}{2\omega\cosh kh}\frac{\partial A^{\pm}}{\partial\xi_1} \tag{3.25}$$

which are induced via $\gamma_{1,1}^{1,\pm}e^{iS_{1,1}^{\pm}}\xrightarrow{\overline{\mathcal{L}}_{\text{flu}}}\gamma f^{\pm}e^{iS_{1,1}^{\pm}}$ and $\gamma_{1,1}^{1,\mp}e^{iS_{1,1}^{\mp}}\xrightarrow{\overline{\mathcal{L}}_{\text{bot}}}\gamma b^{\pm}e^{iS_{1,1}^{\pm}}$, respectively. The generations of B_1^{+}, B_2^{+} and B_3^{+} are described as

$$\begin{gathered}\gamma_{1,1}^{1,+}e^{iS_{1,1}^{+}}\xrightarrow{\mathcal{L}_{\text{sur}}}B_1^{+}\\ \gamma f^{+}e^{iS_{1,1}^{+}}\xrightarrow{\mathcal{L}_{\text{sur}}}B_2^{+}\\ \left(\gamma_{1,1}^{1,+}e^{iS_{1,1}^{+}},\gamma f^{+}e^{iS_{1,1}^{+}}\right)\xrightarrow{\mathcal{L}_{\text{flu}}}B_3^{+}\end{gathered} \tag{3.26}$$

and for D_1^{+}, D_2^{+} and D_3^{+}, we have

$$\begin{gathered}\gamma b^{+}e^{iS_{1,1}^{+}}\xrightarrow{\mathcal{L}_{\text{sur}}}D_1^{+}\\ \left(\gamma_{1,1}^{1,-}e^{iS_{1,1}^{-}}\xrightarrow{\mathcal{L}_{\text{flu}}},\gamma f^{-}e^{iS_{1,1}^{-}}\xrightarrow{\mathcal{L}_{\text{bot}}}\right)B_3^{+}\\ \gamma_{3,1}^{2,+}e^{iS_{3,1}^{+}}\xrightarrow{\mathcal{L}_{\text{bot}}}D_3^{+}\end{gathered} \tag{3.27}$$

The generation of D_1^{+} is presented by $\gamma_{1,1}^{1,-}e^{iS_{1,1}^{-}}\xrightarrow{\overline{\mathcal{L}}_{\text{bot}}}\gamma b^{+}e^{iS_{1,1}^{+}}\xrightarrow{\mathcal{L}_{\text{sur}}}D_1^{+}$. This process is initiated by a first-order reflected wave, $\gamma_{1,1}^{1,-}e^{iS_{1,1}^{-}}$. Subsequently, the reflected wave is further reflected by the positive component of the bottom, e^{2ikx}, resulting in the forward mode $\gamma b^{+}e^{iS_{1,1}^{+}}$. Finally, the wave is temporally modulated at the surface boundary to generate the desired term, D_1^{+}. The detailed generation process of D_1^{+} reveals the impact mechanisms of D_1^{+} on downshifting behaviour, as presented in table 3, which is the combination of the bottom re-reflection effect and the surface modulation effect. Moreover, both the resonant and the non-resonant components of $O\left(\varepsilon^2\right)$ contribute to this downward shift, with the latter, $\gamma_{3,1}^{2,+}e^{iS_{3,1}^{+}}$ of second order, being particularly prominent as the bottom height varies steeper.

The generation of D_2^{+} is more intricate and involves three distinct paths: $\gamma_{1,1}^{1,-}e^{iS_{1,1}^{-}}\xrightarrow{\mathcal{L}_{\text{bot}}}$

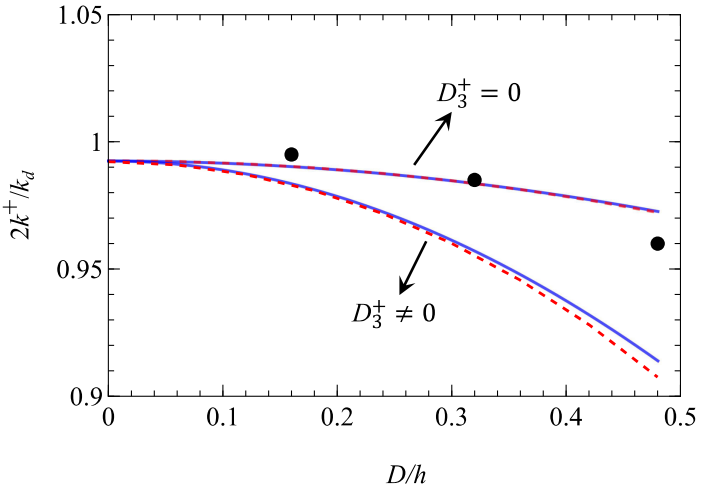

Figure 4: Comparison of wavenumber of the incident wave of the Bragg resonance among the analytical solution of (3.21) (blue solid line), the numerical results of (3.20) (red dashed line) that includes the influence of the non-resonant mode ($D_3^+ \neq 0$) or excludes this mode ($D_3^+ = 0$), and results of Liu et al. (2019) from the MMSE (black dots).

D_2^+, $\gamma_{1,1}^{1,-}e^{iS_{1,1}^-} \xrightarrow{\overline{\mathcal{L}}_{\text{bot}}} \gamma b^+ e^{iS_{1,1}^+} \xrightarrow{\mathcal{L}_{\text{flu}}} D_2^+$ and $\gamma_{1,1}^{1,-}e^{iS_{1,1}^-} \xrightarrow{\overline{\mathcal{L}}_{\text{flu}}} \gamma f^- e^{iS_{1,1}^-} \xrightarrow{\mathcal{L}_{\text{bot}}} D_2^+$, which is a combination of first- and second-order contributions from the fluid and bottom.

D_3^+ is generated by $\gamma_{1,1}^{1,+}e^{iS_{1,1}^+}$, with paths $\gamma_{1,1}^{1,+}e^{iS_{1,1}^+} \xrightarrow{\overline{\mathcal{L}}_{\text{bot}}} \gamma_{3,1}^{2,+}e^{iS_{3,1}^+} \xrightarrow{\mathcal{L}_{\text{bot}}} D_3^+$, indicating that the first-order incident wave is induced by the first-order bottom effect to generate the non-resonant forward wave, $\gamma_{3,1}^{2,+}e^{iS_{3,1}^+}$. This wave is further forced by the second-order bottom effect to strengthen the resonant modes.

To examine the effect of D_3^+ on the frequency downshift, we compare our results with the solutions of Liu et al. (2019), in which the modified mild slope equation (MMSE) was applied to investigate the effect of bottom height on the downshift behaviour of the Bragg resonance. The experimental settings of case-D1 are adopted, with $h = 0.312$ m, $L = 10$ m, $\lambda_d = 1$ m and $N_d = 10$ fixed, with varying bottom amplitude D.

As shown in figure 4, with the increase of bottom amplitude, significant divergence between the present solution and the results of Liu et al. (2019) is observed, which is probably attributed to the influence of the non-resonant wave mode, $\gamma_{3,1}^{2,+}e^{iS_{3,1}^+}$, which was neglected in the MMSE. By setting D_3^+ to zero to eliminate the effect of this non-resonant wave, the present analytical and numerical results show satisfactory agreement with the solutions obtained by the MMSE. This reveals that the non-resonant mode is a dominant factor responsible for the downward shift in the wavenumber of the Bragg resonance for steep bottom amplitude.

3.3.3. *Impact of the bottom amplitude on the magnitude of the Bragg resonance downshift*

The approximate expression for the magnitude of the wave frequency downshift (3.21), which is of a parabolic form, i.e., $\delta \approx \delta_0 + \delta_2$, with $\delta_0 = O(1)$ and $\delta_2 = O\left(D^2\right)$, reveals that with the increase of bottom amplitude D, the parabolic or squared trend of δ is more pronounced than its linear trend since δ_1 (the primary term of D) is always equal to zero. Additionally, a threshold downshift magnitude is observed; for $D \to 0$, δ converges to δ_0, which is negative for finite sandbar lengths ($L < \infty$), indicating that for finite sandbar lengths, any amplitude

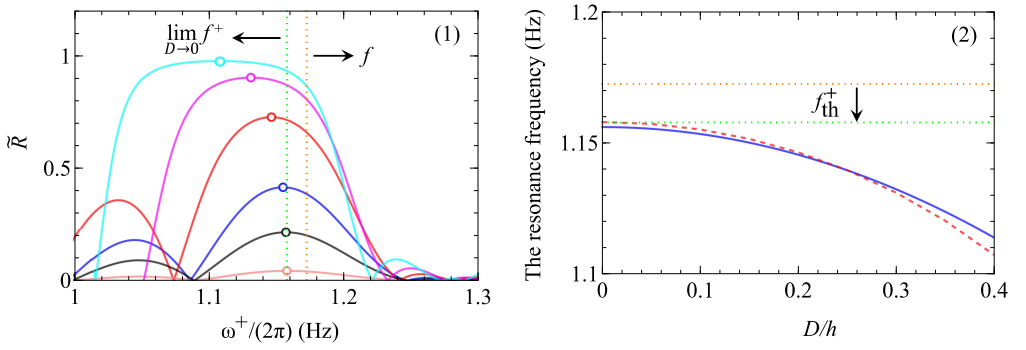

Figure 5: (1) Reflection rate (3.16) versus wave frequency for various D/h values, with circles denoting the peak value, and the solid lines, from top to bottom, represent D/h = 0.4, 0.3, 0.2, 0.1, 0.05, 0.01. (2) Comparison of the analytical solution in (3.21) (blue solid line) and numerical results from (3.20) (red dashed line) on the frequency of the Bragg resonance versus bottom amplitude. Green and orange dotted lines represent the threshold frequency and wave frequency, respectively.

can result in a downward shift, while for $L \to \infty$, where δ_0 tends to 0 , and the downshift threshold is eliminated.

To further examine the theoretical expression of the downshift magnitude and provide further insight into the phenomenon, the solutions of reflection rate and resonance frequency for gradually increased D/h are presented. In case L1, the parameters $h, L, \lambda_d, N_d, k_d$, and k are set to 0.22 m, 2.5 m, 0.5 m, 10, 4π/m, and 2π/m. The reflection rate for various sandbar amplitudes D is then calculated for a range of wave frequencies.

Figure 5 (1) presents the variation of the reflective coefficients with respect to the ratio of the sandbar amplitude D to the water depth h. The shift of the open markers indicates an enhancement of downshift behaviour of the Bragg resonance with the increase of D/h. Conversely, with the decrease of D/h, the frequency of the reflection peaks increases up to a limit of 1.1578 Hz, as shown in in figure 5 (2) (depicted by the green dotted line), with f_{th}^+ denoting the downward shift of the wave frequency to the threshold frequency. This frequency can be obtained both analytically (blue solid line from the theoretical expression (3.21)) and numerically (red dashed line, by conducting the numerical procedure for (3.20)). Overall agreement between the two solutions is observed, confirming the parabolic trend of the Bragg resonance frequency as a function of the bottom amplitude. Additionally, the wave frequency $f = \omega/2\pi = 1.1725$ Hz, which is the frequency without downshift and depicted by the orange dotted line in both figures 5 (1) and (2), is always above the other curves, indicating the downshift behaviour for any sandbar amplitude D. The agreement between the two solutions in figure 5 (2) further demonstrates the hypothesis of the existence of a threshold frequency.

4. The effect of wave nonlinearity

Wave nonlinearity is a key factor that affect wave transformation and reflection by altering wave speed and can cause nonlinear behaviours such as freak waves. In the previous work, we neglected the influence of nonlinearity on Bragg resonance for the convenience of analytical solution. In this section, the full nonlinear ENLS equation are solved numerically, and a brief numerical procedure followed by an investigation of wave nonlinearity impact on wave reflection problems are presented in this part.

4.1. *Solution procedure*

Let $R_{\mathrm{re}}(x), T_{\mathrm{re}}(x)$ and $R_{\mathrm{im}}(x), T_{\mathrm{im}}(x)$ denote the real and imaginary parts of $R(x)$ and $T(x)$, respectively. $A^{\pm}$ can be expressed as

$$A^{+}=A_0\left(T_{\mathrm{re}}(x)+iT_{\mathrm{im}}(x)\right)e^{ik'x-i\omega' t}\quad(0<x<L) \tag{4.1}$$

and

$$A^{-}=A_0\left(R_{\mathrm{re}}(x)+iR_{\mathrm{im}}(x)\right)e^{-ik''x-i\omega' t}\quad(0<x<L). \tag{4.2}$$

Substituting (4.1) and (4.2) into (2.37) and (2.38), and separating real and imaginary items, we have

$$\frac{d\vec{Y}(x)}{dx}=\vec{\wp}(x) \tag{4.3}$$

in which

$$\vec{Y}(x)=\left(R_{\mathrm{re}},R_{\mathrm{im}},T_{\mathrm{re}},T_{\mathrm{im}}\right)^{T}$$

$$\vec{\wp}(x)=\begin{pmatrix} S_3^{+} & 0 & S_4^{+} & 0\\ 0 & -S_3^{+} & 0 & -S_4^{+}\\ S_4^{+} & 0 & S_3^{+} & 0\\ 0 & S_4^{+} & 0 & S_3^{+}\end{pmatrix}^{-1}\left\{-\begin{pmatrix} iS_1^{+}R_{\mathrm{im}}+iS_2^{+}T_{\mathrm{im}}\\ iS_1^{+}R_{\mathrm{re}}+iS_2^{+}T_{\mathrm{re}}\\ -iS_2^{+}R_{\mathrm{im}}-iS_1^{+}T_{\mathrm{im}}\\ iS_2^{+}R_{\mathrm{re}}+iS_1^{+}T_{\mathrm{re}}\end{pmatrix}+\overrightarrow{\wp_n}(x)\right\}, \tag{4.4}$$

and $\overrightarrow{\wp_n}(x)$ is the nonlinear contribution,

$$\overrightarrow{\wp_n}(x)=-iA_0^2\begin{pmatrix} T_{\mathrm{im}}\left\{F_2^{+}\left(R_{\mathrm{im}}^2+R_{\mathrm{re}}^2\right)+F_1^{+}\left(T_{\mathrm{im}}^2+T_{\mathrm{re}}^2\right)\right\}\\ T_{\mathrm{re}}\left\{F_2^{+}\left(R_{\mathrm{im}}^2+R_{\mathrm{re}}^2\right)+F_1^{+}\left(T_{\mathrm{im}}^2+T_{\mathrm{re}}^2\right)\right\}\\ -R_{\mathrm{im}}\left\{F_1^{+}\left(R_{\mathrm{im}}^2+R_{\mathrm{re}}^2\right)+F_2^{+}\left(T_{\mathrm{im}}^2+T_{\mathrm{re}}^2\right)\right\}\\ R_{\mathrm{re}}\left\{F_1^{+}\left(R_{\mathrm{im}}^2+R_{\mathrm{re}}^2\right)+F_2^{+}\left(T_{\mathrm{im}}^2+T_{\mathrm{re}}^2\right)\right\}\end{pmatrix}. \tag{4.5}$$

According to (3.15), the boundary conditions gives,

$$T_{\mathrm{re}}(0)=1, T_{\mathrm{im}}(0)=0, R_{\mathrm{re}}(L)=0, R_{\mathrm{im}}(L)=0. \tag{4.6}$$

For a specific frequency ω' and wave amplitude of incident wave A_0, the nonlinear system of ordinary differential equations (4.3) with boundaries (4.6) forms a well-defined BVP. We adopt a fourth-order Runge-Kutta method with a step size of $\Delta x = L/N_t$, with N_t fixed to 10^4, to discretize the governing equation. x^n is denoted as the discrete points on $[0, L]$, where $x^n = (n-1)\Delta x$, $(1 \leqslant n \leqslant N_t+1)$, and $\vec{Y}(x_n)$ and $\vec{\wp}(x_n)$ are defined as $\vec{Y}^n$ and $\vec{\wp}^n$, respectively. To evaluate the error of the numerical solutions, we introduce the an indicator:

$$\mathrm{err}=\sum_{n=1}^{N_t}\left|\frac{\vec{Y}^{n+1}-\vec{Y}^{n}}{\Delta x}-\vec{\wp}^{n}\right|^2\frac{\Delta x}{L}, \tag{4.7}$$

which represents the global squared error of the numerical solution on $[0, L]$. Each incident wave frequency and wave amplitude correspond to an error. Thus, $\mathrm{err}_{\max}$ can be used to characterize the maximum error

$$\mathrm{err}_{\max}=\max_{A_0,\omega'}\{\mathrm{err}\}. \tag{4.8}$$

By choosing this discrete format, the accuracy of the numerical solutions can be guaranteed, with $\mathrm{err}_{\max} < 10^{-6}$. The reflection coefficient can be obtained by

$$\tilde{R}=\left|R_{\mathrm{re}}(x^1)+iR_{\mathrm{im}}(x^1)\right|. \tag{4.9}$$

Case	h(m)	D/h	k_d(/m)	λ_d(m)	N_d	k(/m)	$2k^+/k_d$	kA_0	$\mathrm{err}_{\max}$
(a)	0.156	0.160	2π	1.0	10	π	$0.85 \sim 1.15$	$0 \sim 0.05$	1.3×10^{-7}
(b)	0.780	0.160	2π	0.5	10	π	$0.85 \sim 1.15$	$0 \sim 0.10$	1.3×10^{-7}

Table 4: Incident wave and bottom conditions.

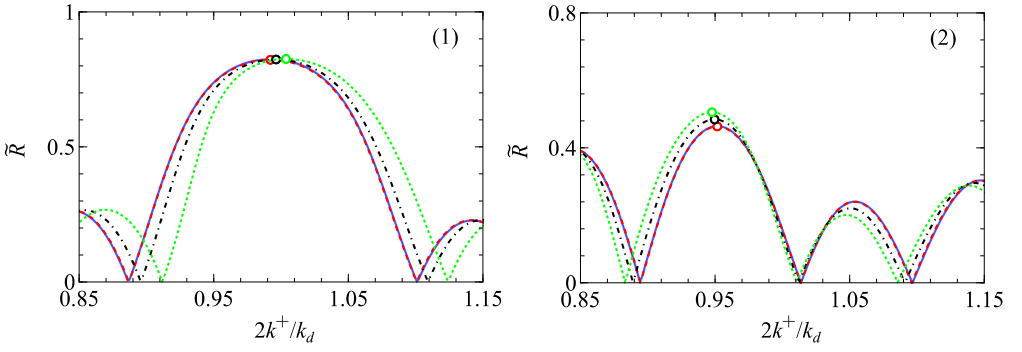

Figure 6: Comparisons of reflection rate versus wavenumber of the incident wave for (1) case (a) among linear analytical solution in (3.16) (blue solid line), numerical solutions for $kA_0 = 0$ (red dashed line), 0.03 (black dot-dashed line) and 0.05 (green dotted line); (2) case (b) among linear analytical solution in (3.16) (blue solid line), numerical solutions for $kA_0 = 0$ (red dashed line), 0.07 (black dot-dashed line), 0.10 (green dotted line).

The wavenumbers of the incident and reflected waves can be expressed as:

$$k^+ = k - \frac{iB_1^+ (\omega')^2 - \omega'}{S_4^+} + \frac{iF_1^+ A_0^2}{S_4^+} + \frac{iF_2^+ A_0^2 \tilde{R}^2}{S_4^+}$$

$$k^- = k - \frac{iB_1^+ (\omega')^2 - \omega'}{S_4^+} + \frac{iF_1^+ A_0^2 \tilde{R}^2}{S_4^+} + \frac{iF_2^+ A_0^2}{S_4^+}, \tag{4.10}$$

which include the information for the wave amplitude of the incident wave and reflected wave by A_0 and $A_0\tilde{R}$, respectively.

4.2. *Upward and downward shifts of the Bragg resonance*

To explore the impact of wave nonlinearity on reflection, we adopt the setup of experimental case D1, with the exception of the water depth and sandbar amplitude. We select a range of water depths, all with a fixed bottom steepness of $D/h = 0.16$. The parameters of our numerical solutions are detailed in table 4, with the maximum error of each displayed in the last column.

As shown in figures 6 (1) and (2), the analytical solution and the numerical solution are completely coincident for $kA_0 = 0$, demonstrating the accuracy of the numerical results of the reflection rate. Besides, the numerical results show that the increase in wave steepness yields a slight increase in the maximum reflection for both cases. Figure 6 (1) shows that as the wave steepness increases, the wavenumber of the Bragg resonance shifts upward. Figures 7 (1) and (2) depict the relation between the incident wavenumber and the wave steepness. For case (a), as illustrated in figure 7 (1), in which intensifying the wave steepness significantly increases the wavenumber of the Bragg resonance. For case (b), which has a

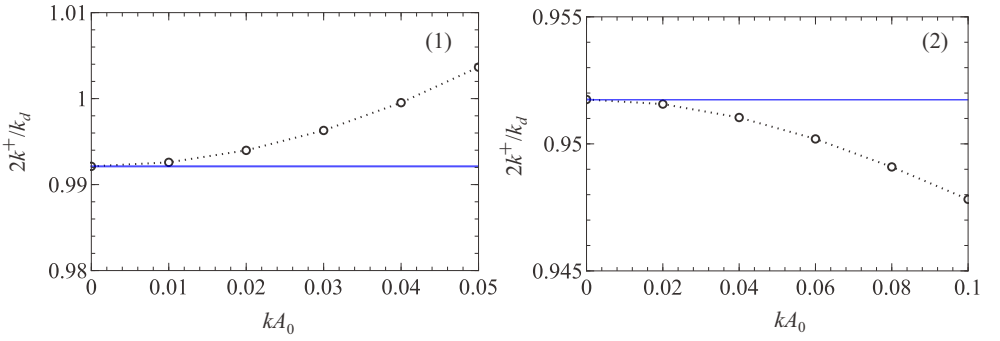

Figure 7: The linear analytical (blue solid lines) and numerical solutions (black dotted lines) for wavenumber of the incident wave of the Bragg resonance for different wave steepness for (1): cases (a) and (2): case (b).

Case	k_d(/m)	λ_d(m)	N_d	kh	D/h	kA_0	$\mathrm{err}_{\max}$
(a)	2π	1.0	30	1.157	0.16×10^{-5}	$0\sim0.06$	1.7×10^{-13}
(b)	2π	1.0	30	1.159	0.16×10^{-5}	$0\sim0.06$	1.6×10^{-13}

Table 5: Incident wave and bottom conditions.

larger water depth, the wavenumber of the Bragg resonance decreases monotonically with increasing wave steepness, as demonstrated in figure 7 (2). The numerical results reveals that the wave nonlinearity can cause different frequency shifting characteristics in the Bragg resonance under different water depth conditions.

To gain a better understanding of this phenomenon, the Bragg resonance criterion is applied. According to previous analysis, for a sufficiently large bottom length and extremely small bottom amplitude, the criterion, which indicates the maximum reflection, is accurate

$$k^+ + k^- = k_d. \tag{4.11}$$

Combining this criterion with dispersion relation (4.10) gives

$$\frac{2k^+}{k_d} = 1 + \frac{k^+ - k^-}{k_d} = 1 + \frac{iF_1^+ - iF_2^+}{S_4^+ k_d} A_0^2 \left(1 - \tilde{R}^2\right), \tag{4.12}$$

in which iF_1^+ and iF_2^+ are the self-phase and cross-phase modulation coefficients (Onorato et al. 2006), respectively. Thus, we have

$$\frac{iF_1^+ - iF_2^+}{S_4^+ k_d} = \begin{cases} > 0, & kh < 1.158 \\ < 0, & kh > 1.158 \end{cases} \tag{4.13}$$

which shows a monotonic relationship between $2k^+/k_d$ and A_0. For $kh < 1.158$, $2k^+/k_d$ shifts upward with increasing wave amplitude A_0, where $k^+ > k^-$, and for $kh > 1.158$, $2k^+/k_d$ shows downshift behaviour with increasing A_0, where $k^+ < k^-$. Therefore, the different behaviour is probably linked to the discrepancy between the incident and reflected wavenumbers, which is induced by wave nonlinearity.

To verify the above hypothesis, we conduct numerical examples in the vicinity of $kh = 1.158$ by adopting different water depths for further examination. To satisfy the Bragg criterion in (4.11), sufficient large length for the sandbars and sufficient small D are required.

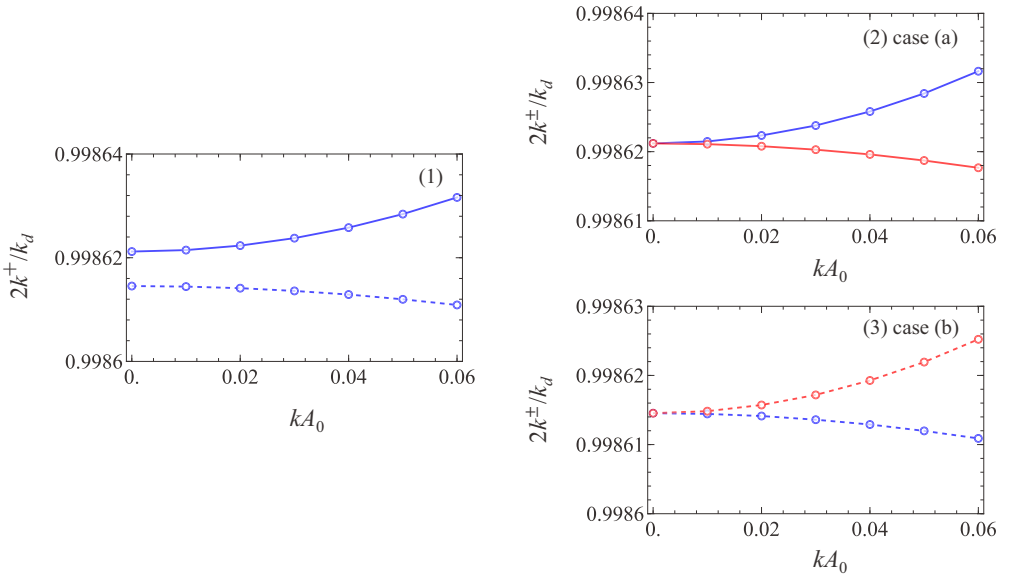

Figure 8: (1): The incident wavenumber of the Bragg resonance versus wave steepness for case (a) (blue solid line) and case (b) (blue dashed line). (2) and (3): The incident wavenumbers $2k^+/k_d$ (blue lines) and reflected wavenumber $2k^-/k_d$ (red lines) at the Bragg resonance versus wave steepness for cases (a) and (b), respectively.

The detailed parameters and maximum error at resonance for different water depths are shown in table 5.

Figure 8 (1) shows the relations between the incident wavenumber of the Bragg resonance and wave steepness for case (a), $kh = 1.157$, and case (b), $kh = 1.159$, which illustrates completely opposite behaviour of the peak reflection in the vicinity of $kh = 1.158$, with the corresponding incident and reflected wavenumbers at the Bragg resonance displayed in figures 8 (2) and (3) for case (a) and case (b), in which the different behaviour is due to the sign variation in the incident and reflected wavenumber differences around a certain critical $kh = 1.158$. Essentially, the change of water depth causes an alteration in wave modulation effect, namely, as the water depth increases, the waves change from being dominated by the self-modulation effect $\left(iF_1^+ > iF_2^+\right)$ to being dominated by the cross-modulation effect $\left(iF_2^+ > iF_1^+\right)$. Note that while the existence of the behaviour is confirmed and explained by the Bragg criterion in the extreme case (L is sufficiently large, and $D \to 0$), the critical kh is not constantly equal to 1.158 , and the value relies on specific bottom circumstances according to our study, which requires further investigation.

5. Conclusion

In this work, the ENLS equations are derived by employing the multiple-scale expansion method to describe wave scattering by sinusoidal sandbars. A closed-form solution is established by solving the linearized ENLS equations and a theoretical formula for the downshift magnitude of the resonance frequency is proposed. The factors that influence the downshift of the Bragg resonance are examined and the underlying mechanisms are revealed. Finally, fully nonlinear ENLS equations are solved numerically to investigate the effect of wave nonlinearity on wave reflection. The main conclusions are drawn as follows:

1. Among the effects of high-order bottom, high-order dispersion and nonlinear wave-

wave interaction on Bragg scattering, the high-order bottom effect is the major cause of the downshift behaviour, attributed to the combination of the re-reflection of waves and the surface modulation effect. Besides, the interaction between the forward non-resonant mode and sinusoidal sandbars also plays an important role in causing downshift behaviour, especially when the sandbar amplitude varies steeply, where a significant increase in the downward shift appears that leads to an underestimation of the downshift behaviour by the MMSE.

2. An analytical formula for the wave frequency downshift is presented that exhibits a parabolic form with respect to the amplitude and length of sandbars, which remains valid even if the bar length approaches infinity. As the bar amplitude tends to zero, the magnitude of the frequency downshift converges to a negative threshold. This phenomenon is caused by the finite length of the sandbars and vanishes as the length approaches to infinity. In addition, an expression for the wavenumber of the reflection peaks is derived via dispersion relation, which degenerates to the standard Bragg law as the sandbar length approaches to infinity and the bar amplitude approaches to zero, validating the standard Bragg law under this condition.

3. The nonlinearity of the waves has been observed to cause a shift of the Bragg resonance, with both an upward and a downward in behaviour, attributed to the discrepancy between the wavenumbers of the incident and reflected waves, which is highly represented by kh. Specifically, when kh is above a critical value (equal to 1.158 under limiting conditions), the increase of wave nonlinearity causes a significant downshift of the Bragg resonance, where it is dominated by the cross-modulation effect with the reflected wavenumber larger than that of the incident wave. With the decreases of kh, the waves gradually transition from being cross-modulated-dominated to selfmodulated-dominated, as a result, the incident wavenumber gradually increases and becomes larger than the reflected wavenumber, together with the gradually change of Bragg resonance frequency from downshift to upshift. Therefore, when kh is smaller than the critical value, the enhancement of wave nonlinearity triggers an upshift behaviour. Although we demonstrate the existence of the critical value that equals to 1.158 under extreme conditions, the critical value will change with the amplitude and length of sandbars, which necessitates further investigations.

Acknowledgements. This work is supported, in part, by the National Natural Science Foundation of China (Grant No. 52031002) and the Ministry of Science and Technology of the People's Republic of China (MST) under the High-level Overseas Talents introducing project (Grant No. G20200023001).

Declaration of interests. The authors declare that they have no known competing financial interests or personal relationships that could have appeared to influence the work reported in this paper.

Author ORCIDs. Haiqi Fang, https://orcid.org/0009-0005-7182-5004.

Author contributions. Haiqi Fang: Methodology, Validation, Formal analysis, Writing – original draft, manuscript preparation. Lian Tang: Formal analysis, Writing – review and editing, specifically critical review, commentary or revision. Pengzhi Lin: Conceptualization, Supervision. All authors reviewed the results and approved the final version of the manuscript.

6. Appendix

6.1. *Appendix A. Solving procedure of the jth order problem for ϕ_j*

In general, we consider the j th order problem for ϕ_j, defined by the following equations,

$$\frac{\partial^2 \phi_j}{\partial x^2} + \frac{\partial^2 \phi_j}{\partial z^2} = T_j \quad (-h < z < 0) \tag{6.1}$$

$$\frac{\partial^2 \phi_j}{\partial t^2} + g\frac{\partial \phi_j}{\partial z} = P_j \quad (z = 0) \tag{6.2}$$

$$\frac{\partial \phi_j}{\partial z} = Q_j \quad (z = -h) \tag{6.3}$$

ϕ_j is assumed to be expressed as series form in terms of multiple harmonics,

$$\phi_j = \gamma_{0,0}^{j,+} + \sum_{\substack{mn=0 \\ m+n>0}} \left(\gamma_{m,n}^{j,+} e^{iS_{m,n}^{+}} + \text{C. C.} \right) + \sum_{m=1}^{\infty} \sum_{n=1}^{\infty} \left(\gamma_{m,n}^{j,+} e^{iS_{m,n}^{+}} + \gamma_{m,n}^{j,-} e^{iS_{m,n}^{-}} + \text{C. C.} \right) \tag{6.4}$$

where $\gamma_{m,n}^{j,\pm} = \gamma_{m,n}^{j,\pm}(z, \xi_1, \tau_1, \xi_2, \tau_2)$ are functions corresponding to $e^{iS_{m,n}^{\pm}}$ for the j th order problem. Substituting (6.4) to (6.1) - (6.3) and separating different orders of harmonics, $S_{m,n}^{\pm}$, a set of ordinary differential equations for $\gamma_{m,n}^{j,\pm}$ can be obtained.

$$\left(\frac{\partial^2}{\partial z^2} - m^2 k^2 \right) \gamma_{m,n}^{j,\pm} = T_{m,n}^{j,\pm} \quad (-h < z < 0) \tag{6.5}$$

$$g \frac{\partial \gamma_{m,n}^{j,\pm}}{\partial z} - n^2 \omega^2 \gamma_{m,n}^{j,\pm} = P_{m,n}^{j,\pm} \quad (z = 0) \tag{6.6}$$

$$\frac{\partial \gamma_{m,n}^{j,\pm}}{\partial z} = Q_{m,n}^{j,\pm} \quad (z = -h) \tag{6.7}$$

The method of solving (6.5) - (6.7) is highly dependent on the values of the parameters m and n. For the j th-order problem, the solutions of $T_{m,n}^{j,\pm}$, etc., differ depending on whether mn is equal to 1 or not. In the case that $mn \neq 1$, the solutions of $\gamma_{m,n}^{j,\pm}$ are non-singular, obtained directly by solving the boundary value problem. Conversely, when $mn = 1$, the equations become singular, thereby requiring two additional solvability conditions to be satisfied to guarantee the existence of the solution of $\gamma_{m,n}^{j,\pm}$.

6.1.1. *For $mn \neq 1$*

When $mn \neq 1$, the non-homogeneous equation with non-zero boundary conditions can be linearly decomposed into two distinct problems. The first is a homogeneous equation, with two non-zero boundary conditions, and the other a non-homogeneous equation with two zero boundary conditions. Representing each problem is $\gamma_{m,n}^{j,\pm}$, with $\bar{\gamma}_{m,n}^{j,\pm}$ being the solution for the homogeneous equation and $\bar{\bar{\gamma}}_{m,n}^{j,\pm}$ for the non-homogeneous.

$$\gamma_{m,n}^{j,\pm} = \bar{\gamma}_{m,n}^{j,\pm} + \bar{\bar{\gamma}}_{m,n}^{j,\pm} \tag{6.8}$$

For $\bar{\gamma}_{m,n}^{j,\pm}$, we have

$$\left(\frac{\partial^2}{\partial z^2} - m^2 k^2 \right) \bar{\gamma}_{m,n}^{j,\pm} = 0 \quad (-h < z < 0) \tag{6.9}$$

$$g \frac{\partial \bar{\gamma}_{m,n}^{j,\pm}}{\partial z} - n^2 \omega^2 \bar{\gamma}_{m,n}^{j,\pm} = P_{m,n}^{j,\pm} \quad (z = 0) \tag{6.10}$$

$$\frac{\partial \bar{\gamma}_{m,n}^{j,\pm}}{\partial z} = Q_{m,n}^{j,\pm} \quad (z = -h) \tag{6.11}$$

The general solution of (6.9) is $\bar{\gamma}_{m,n}^{j,\pm} = \bar{C}_1 \cosh mk(z+h) + \bar{C}_2 \sinh mk(z+h)$, and $\bar{C}_1$ and $\bar{C}_2$ are two arbitrary complexes, determined by two boundaries, which can be uniquely ensured after substituting the general solution of $\bar{\gamma}_{m,n}^{j,\pm}$ to (6.10) and (6.11). The simplified solution

for $\bar{\gamma}^{j,\pm}_{m,n}$ is derived,

$$\bar{\gamma}^{j,\pm}_{m,n} = \frac{P^{j,\pm}_{m,n}}{gmk\tanh mkh - n^2\omega^2}\frac{\cosh mk(z+h)}{\cosh mkh} + Q^{j,\pm}_{m,n}\left\{\frac{\sinh mk(z+h)}{mk} + \frac{n^2\omega^2\tanh mkh - gmk}{gm^2k^2\tanh mkh - mkn^2\omega^2}\cosh mk(z+h)\right\} \tag{6.12}$$

The second problem is expressed as follows,

$$\left(\frac{\partial^2}{\partial z^2} - m^2k^2\right)\bar{\bar{\gamma}}^{j,\pm}_{m,n} = T^{j,\pm}_{m,n} \quad (-h < z < 0) \tag{6.13}$$

$$g\frac{\partial\bar{\bar{\gamma}}^{j,\pm}_{m,n}}{\partial z} - n^2\omega^2\bar{\bar{\gamma}}^{j,\pm}_{m,n} = 0 \quad (z = 0) \tag{6.14}$$

$$\frac{\partial\bar{\bar{\gamma}}^{j,\pm}_{m,n}}{\partial z} = 0 \quad (z = -h) \tag{6.15}$$

We first multiply (6.13) by $\psi^{\pm}_m$ and integrate from $-h$ to z, the following relation is obtained

$$\int_{-h}^{z}\left(\frac{\partial^2\bar{\bar{\gamma}}^{j,\pm}_{m,n}}{\partial z^2} - m^2k^2\bar{\bar{\gamma}}^{j,\pm}_{m,n}\right)\psi^{\pm}_m dz = \int_{-h}^{z} T^{j,\pm}_{m,n}\psi^{\pm}_m dz \tag{6.16}$$

in which $\psi^{\pm}_m = \cosh mk(z+h)$. After conducting the divisional integral formula and apply the Neumann boundary at $z = -h$, a first-order differential equation is obtained

$$\frac{\partial\bar{\bar{\gamma}}^{j,\pm}_{m,n}}{\partial z} - (mk\tanh mkh)\bar{\bar{\gamma}}^{j,\pm}_{m,n} = \operatorname{sech} mk(z+h)\int_{-h}^{z} T^{j,\pm}_{m,n}\psi^{\pm}_m dz, \tag{6.17}$$

which can be further solved for $\bar{\bar{\gamma}}^{j,\pm}_{m,n}$,

$$\bar{\bar{\gamma}}^{j,\pm}_{m,n} = \left(\mathcal{F}_{m,n}\left(z, T^{j,\pm}_{m,n}\right) + \bar{\bar{C}}_1\right)\cosh mk(z+h), \tag{6.18}$$

where $\mathcal{F}_{m,n}\left(z, T^{j,\pm}_{m,n}\right)$ is a double integral over z, including the forcing term $T^{j,\pm}_{m,n}$:

$$\mathcal{F}_{m,n}\left(z, T^{j,\pm}_{m,n}\right) = \int_{-h}^{z}\int_{-h}^{\rho}[\operatorname{sech} mk(\rho+h)]^2\cosh mk(\sigma+h)T^{j,\pm}_{m,n}(\sigma)d\sigma d\rho. \tag{6.19}$$

$\bar{\bar{C}}_1$ is a complex to be determined by the remaining Robbin boundary at $z = 0$. Substituting (6.18) to (6.14), then $\bar{\bar{C}}_1$ can be uniquely determinded

$$\bar{\bar{C}}_1 = -\mathcal{F}_{m,n}\left(0, T^{j,\pm}_{m,n}\right) + \frac{g\mathcal{F}'_{m,n}\left(0, T^{j,\pm}_{m,n}\right)}{n^2\omega^2 - gmk\tanh mkh}, \tag{6.20}$$

which, combined with (6.18), the solution for $\frac{\partial\bar{\bar{\gamma}}^{j,\pm}_{m,n}}{\partial z}$ is obtained

$$\bar{\bar{\gamma}}^{j,\pm}_{m,n} = \left[\mathcal{F}_{m,n}\left(z, T^{j,\pm}_{m,n}\right) - \mathcal{F}_{m,n}\left(0, T^{j,\pm}_{m,n}\right) + \frac{g\mathcal{F}'_{m,n}\left(0, T^{j,\pm}_{m,n}\right)}{n^2\omega^2 - gmk\tanh mkh}\right]\cosh mk(z+h) \tag{6.21}$$

Thus, the BVP for the harmonics $S^{\pm}_{m,n}$at jth order is solved, giving the solution for $\gamma^{j,\pm}_{m,n}$ in the case of $mn \neq 1$.

$$\begin{aligned}\bar{\gamma}^{j,\pm}_{m,n} &= \frac{P^{j,\pm}_{m,n}}{gmk\tanh mkh - n^2\omega^2}\cosh mk(z+h)\\ &+Q^{j,\pm}_{m,n}\left\{\frac{\sinh mk(z+h)}{mk}+\frac{n^2\omega^2\tanh mkh - gmk}{gm^2k^2\tanh mkh - mkn^2\omega^2}\cosh mk(z+h)\right\}\\ &+\left[\mathcal{F}_{m,n}\left(z,T^{j,\pm}_{m,n}\right)-\mathcal{F}_{m,n}\left(0,T^{j,\pm}_{m,n}\right)+\frac{g\mathcal{F}'_{m,n}\left(0,T^{j,\pm}_{m,n}\right)}{n^2\omega^2 - gmk\tanh mkh}\right]\cosh mk(z+h)\end{aligned} \tag{6.22}$$

6.1.2. *For $mn = 1$*

For the case of $mn = 1$ or $m = n = 1$, the solution for $\gamma^{j,\pm}_{1,1}$ displayed in (6.22) is subjected to divergence due to the dispersion relation. Here, $\psi^{\pm}$ represent the homogenous solutions of (6.5) - (6.7). Multiplying (6.5) by $\psi^{\pm}$ and integrating it between $-h$ and 0, the Green Formula can be applied in accordance with the divisional integral formula, thereby ensuring the solvability of the BVP at $O\left(\varepsilon^j\right)$ for $\gamma^{j,\pm}_{1,1}$

$$\int_{-h}^{0}\left\{\left(\frac{\partial^2\gamma^{j,\pm}_{1,1}}{\partial z^2}-k^2\gamma^{j,\pm}_{1,1}\right)\psi^{\pm}-\left(\frac{\partial^2\psi^{\pm}}{\partial z^2}-k^2\psi^{\pm}\right)\gamma^{j,\pm}_{1,1}\right\}dz=\left(\psi^{\pm}\frac{\partial\gamma^{j,\pm}_{1,1}}{\partial z}-\gamma^{j,\pm}_{1,1}\frac{\partial\psi^{\pm}}{\partial z}\right)\Bigg|_{-h}^{0}. \tag{6.23}$$

Then the simplified solvability condition is expressed as

$$\int_{-h}^{0}T^{j,\pm}_{1,1}\psi^{\pm}dz = g^{-1}P^{j,\pm}_{1,1}\psi^{\pm}\Big|_{z=0} - Q^{j,\pm}_{1,1}\psi^{\pm}\Big|_{z=-h}, \tag{6.24}$$

if the solvability condition (6.24) holds, then the existence of solutions for $\gamma^{j,\pm}_{1,1}$ can be ensured. Thus, the linear differential equation, (6.5), combined with the Neumann boundary condition at $z = -h$, (6.7), is solved for $\gamma^{j,\pm}_{1,1}$,

$$\int_{-h}^{0}T^{j,\pm}_{1,1}\psi^{\pm}dz = g^{-1}P^{j,\pm}_{1,1}\psi^{\pm}\Big|_{z=0} - Q^{j,\pm}_{1,1}\psi^{\pm}\Big|_{z=-h}, \tag{6.25}$$

where the general solution of (6.25) can be indicated by the first term on the righthand side, where C_1 is an arbitrary complex. The third term in (6.7) arises from the non-zero boundary at $z = -h$. In the case of $mn \neq 1$, the process of solving is analogous to the first problem, as depicted by (6.13) - (6.18). The distinguishing factor is that the Robin boundary condition, (6.6), is no longer applicable, thus preventing the determination of the complex C_1. However, the general solution can be included into the ϕ_1 component, which can be disregarded in high-order problems, with $C_1 = 0$ being imposed in order to guarantee a unique answer for $\gamma^{j,\pm}_{1,1}$,

$$\gamma^{j,\pm}_{1,1} = \mathcal{F}_{1,1}\left(z,T^{j,\pm}_{m,n}\right)\cosh k(z+h) + k^{-1}Q^{j,\pm}_{1,1}\sinh k(z+h) \tag{6.26}$$

and $\mathcal{F}_{1,1}\left(z,T^{j,\pm}_{m,n}\right)$ is defined in (6.19). It is worth indicating that for any $T^{j,\pm}_{1,1}$, (6.25) gives the exact solution for $\gamma^{j,\pm}_{1,1}$, with a double integration to be determined, which is related to the functional form of $T^{j,\pm}_{1,1}$.

Particularly, if $T^{j,\pm}_{1,1}$ is the product of $\cosh k(z+h)$ and a constant μ, $T^{j,\pm}_{1,1} = \mu\cosh k(z+h)$,

the double integration in $\mathcal{F}_{1,1}(z)$ can be solved analytically, resulting in

$$\mathcal{F}_{1,1}(z) = \frac{\mu(z+h)}{2k}\tanh k(z+h) \tag{6.27}$$

Thus, under this special case, the analytical expression for $\gamma_{1,1}^{j,\pm}$ is rewritten as follows.

$$\gamma_{1,1}^{j,\pm} = \left(\frac{\mu}{2k}(z+h) + \frac{1}{k}Q_{1,1}^{j,\pm}\right)\sinh k(z+h) \tag{6.28}$$

6.2. *Appendix B. Expressions for coefficients*

Expressions for T_2, P_2, Q_2 and R_2

$$T_2 = -2\frac{\partial^2\phi_1}{\partial x\partial\xi_1} = T_{1,1}^{2,+}e^{iS^+} + T_{1,1}^{2,-}e^{iS^-} + \text{C. C.}$$

$$\begin{aligned}P_2 &= -2\frac{\partial^2\phi_1}{\partial t\partial\tau_1} - \frac{\partial\eta_1}{\partial t}\frac{\partial^2\phi_1}{\partial z\partial t} - \frac{\partial\phi_1}{\partial z}\frac{\partial^2\phi_1}{\partial z\partial t} - \eta_1\frac{\partial^3\phi_1}{\partial z\partial t^2} - g\eta_1\frac{\partial^2\phi_1}{\partial z^2} + \frac{\partial\eta_1}{\partial x}\frac{\partial\phi_1}{\partial x} - \frac{\partial\phi_1}{\partial x}\frac{\partial^2\phi_1}{\partial x\partial t}\\ &= P_{1,1}^{2,+}S_{1,1}^{+} + P_{1,1}^{2,-}S_{1,1}^{-} + P_{0,2}^{2,+}S_{0,2}^{+} + P_{2,2}^{2,+}S_{2,2}^{+} + P_{2,2}^{2,-}S_{2,2}^{-} + \text{C. C.}\end{aligned}$$

$$Q_2 = -\sigma\frac{\partial^2\phi_1}{\partial z^2} + \frac{\partial\sigma}{\partial x}\frac{\partial\phi_1}{\partial x} = Q_{1,1}^{2,+}e^{iS^+} + Q_{1,1}^{2,-}e^{iS^-} + Q_{3,1}^{2,+}e^{iS_{3,1}^+} + Q_{3,1}^{2,-}e^{iS_{3,1}^-} + \text{C. C.}$$

$$\begin{aligned}R_2 &= -\frac{1}{g}\left[\frac{\partial\phi_2}{\partial t} + \frac{\partial\phi_1}{\partial\tau_1} + \eta_1\frac{\partial^2\phi_1}{\partial z\partial t} + \frac{1}{2}\left(\frac{\partial\phi_1^2}{\partial x} + \frac{\partial\phi_1^2}{\partial z}\right)\right]\\ &= R_{0,0}^{2,+} + \left(R_{1,1}^{2,+}S_{1,1}^{+} + R_{1,1}^{2,-}S_{1,1}^{-} + R_{0,2}^{2,+}S_{0,2}^{+}R_{2,0}^{2,-}S_{2,0}^{-} + R_{2,2}^{2,+}S_{2,2}^{+} + R_{2,2}^{2,-}S_{2,2}^{-} + \text{C. C.}\right)\end{aligned}$$

Expressions for $T_{m,n}^{2,\pm}, P_{m,n}^{2,\pm}, Q_{m,n}^{2,\pm}$ and $R_{m,n}^{2,\pm}$

$$T_{1,1}^{2,+} = -\frac{gk}{\omega}\frac{\cosh k(z+h)}{\cosh kh}\frac{\partial A^+}{\partial\xi_1}$$

$$T_{1,1}^{2,-} = \frac{gk}{\omega}\frac{\cosh k(z+h)}{\cosh kh}\frac{\partial A^-}{\partial\xi_1}$$

$$P_{1,1}^{2,+} = g\frac{\partial A^+}{\partial\tau_1}$$

$$P_{1,1}^{2,-} = g\frac{\partial A^-}{\partial\tau_1}$$

$$P_{0,2}^{2,+} = -\frac{i\left(3\omega^4 + g^2k^2\right)}{2\omega}A^+A^-$$

$$P_{2,2}^{2,+} = -\frac{3i\left(\omega^4 - g^2k^2\right)}{4\omega}\left(A^+\right)^2$$

$$P_{2,2}^{2,-} = -\frac{3i\left(\omega^4 - g^2k^2\right)}{4\omega}\left(A^-\right)^2$$

$$Q_{1,1}^{2,+} = -\frac{iDgk^2\operatorname{sech}kh}{4\omega}A^-$$

$$Q_{1,1}^{2,-} = -\frac{iDgk^2\operatorname{sech}kh}{4\omega}A^+$$

$$Q_{3,1}^{2,+} = \frac{3iDgk^2\operatorname{sech}kh}{4\omega}A^+$$

$$Q_{3,1}^{2,-} = \frac{3iDgk^2\operatorname{sech}kh}{4\omega}A^-$$

$$R^{2,+}_{0,0} = \frac{\omega^4 - g^2k^2}{4g\omega^2}\left[A^+\left(A^+\right)^* + A^-\left(A^-\right)^*\right] - \frac{1}{g}\frac{\partial B}{\partial \tau_1} - \frac{1}{g}\frac{\partial \phi_2}{\partial t}$$

$$R^{2,+}_{1,1} = \frac{i}{2\omega}\frac{\partial A^+}{\partial \tau_1}$$

694

$$R^{2,-}_{1,1} = \frac{i}{2\omega}\frac{\partial A^-}{\partial \tau_1}$$

$$R^{2,+}_{0,2} = \frac{3\omega^4 + g^2k^2}{4g\omega^2}A^+A^-$$

$$R^{2,+}_{2,0} = \frac{\omega^4 + g^2k^2}{4g\omega^2}A^+\left(A^-\right)^*$$

695

$$R^{2,+}_{2,2} = \frac{3\omega^4 - g^2k^2}{8g\omega^2}\left(A^+\right)^2$$

$$R^{2,-}_{2,2} = \frac{3\omega^4 - g^2k^2}{8g\omega^2}\left(A^-\right)^2$$

696 **Expressions for $\gamma^{2,\pm}_{m,n}$ and $\beta^{2,\pm}_{m,n}$**

$$\gamma^{2,+}_{1,1} = -\frac{g\sinh k(z+h)}{4\omega\cosh kh}\left[2(z+h)\frac{\partial A^+}{\partial \xi_1} + ikDA^-\right]$$

$$\gamma^{2,-}_{1,1} = \frac{g\sinh k(z+h)}{4\omega\cosh kh}\left[2(z+h)\frac{\partial A^-}{\partial \xi_1} - ikDA^+\right]$$

$$\gamma^{2,+}_{2,2} = -\frac{3i\left(\omega^4 - g^2k^2\right)^2}{16\omega^7\,\mathrm{sech}\,2k(z+h)}\left(A^+\right)^2$$

697

$$\gamma^{2,-}_{2,2} = -\frac{3i\left(\omega^4 - g^2k^2\right)^2}{16\omega^7\,\mathrm{sech}\,2k(z+h)}\left(A^-\right)^2$$

$$\gamma^{2,+}_{0,2} = \frac{i\left(3\omega^4 + g^2k^2\right)}{8\omega^3}A^+A^-$$

$$\gamma^{2,+}_{3,1} = \frac{3iDgk^2\,\mathrm{sech}\,kh}{4\omega}\frac{3gk\cosh 3kz + \omega^2\sinh 3kz}{3k\omega^2\cosh 3kh - 9gk^2\sinh 3kh}A^+$$

$$\gamma^{2,-}_{3,1} = \frac{3iDgk^2\,\mathrm{sech}\,kh}{4\omega}\frac{3gk\cosh 3kz + \omega^2\sinh 3kz}{3k\omega^2\cosh 3kh - 9gk^2\sinh 3kh}A^-$$

$$\beta^{2,+}_{0,0} = \frac{\omega^4 + g^2k^2}{4g\omega^2}\left[A^+\left(A^+\right)^* + A^-\left(A^-\right)^*\right] - \frac{1}{g}\frac{\partial B}{\partial \tau_1}$$

698

$$\beta^{2,+}_{2,0} = \frac{\omega^4 + g^2k^2}{4g\omega^2}A^+\left(A^-\right)^*$$

$$\beta^{2,+}_{1,1} = \frac{1}{4gk\omega}\left[2i\left(gk\frac{\partial A^+}{\partial \tau_1} - h\omega^3\frac{\partial A^+}{\partial \xi_1}\right) + Dk\omega^3A^-\right]$$

$$\beta^{2,-}_{1,1} = \frac{1}{4gk\omega}\left[2i\left(gk\frac{\partial A^-}{\partial \tau_1} + h\omega^3\frac{\partial A^-}{\partial \xi_1}\right) + Dk\omega^3A^+\right]$$

699

$$\beta^{2,+}_{2,2} = -\frac{gk^2\left(\omega^4 - 3g^2k^2\right)}{8\omega^6}\left(A^+\right)^2$$

$$\beta^{2,-}_{2,2} = -\frac{gk^2\left(\omega^4 - 3g^2k^2\right)}{8\omega^6}\left(A^-\right)^2$$

$$\beta_{3,1}^{2,+} = \frac{3D\left(\omega^4 + g^2k^2\right)^2}{32g^3k^2\omega^2}A^+$$

$$\beta_{3,1}^{2,-} = \frac{3D\left(\omega^4 + g^2k^2\right)^2}{32g^3k^2\omega^2}A^-$$

Expressions for T_3, P_3, Q_3 and R_3

$$T_3 = -\frac{\partial^2\phi_1}{\partial\xi_1^2} - 2\frac{\partial^2\phi_1}{\partial x\partial\xi_2} - 2\frac{\partial^2\phi_2}{\partial x\partial\xi_1}$$

$$Q_3 = \frac{\partial\sigma}{\partial x}\frac{\partial\phi_1}{\partial\xi_1} - \sigma\frac{\partial^2\phi_2}{\partial z^2} - \frac{1}{2}\sigma^2\frac{\partial^3\phi_1}{\partial z^3} + \frac{\partial\sigma}{\partial x}\frac{\partial\phi_2}{\partial x} + \sigma\frac{\partial\sigma}{\partial x}\frac{\partial^2\phi_1}{\partial x\partial z}$$

$$R_3 = -\frac{1}{g}\left[\frac{\partial\phi_1}{\partial\tau_2} + \frac{\partial\phi_2}{\partial\tau_1} + \frac{\partial\phi_3}{\partial t} + \frac{\partial\phi_1}{\partial z}\frac{\partial\phi_2}{\partial z} + \eta_1\frac{\partial^2\phi_1}{\partial z\partial\tau_1} + \eta_2\frac{\partial^2\phi_1}{\partial z\partial t} + \eta_1\frac{\partial^2\phi_2}{\partial z\partial t}\right.$$
$$\left. + \eta_1\frac{\partial\phi_1}{\partial z}\frac{\partial^2\phi_1}{\partial z^2} + \frac{1}{2}\eta_1^2\frac{\partial^3\phi_1}{\partial t\partial z^2} + \frac{\partial\phi_1}{\partial x}\frac{\partial\phi_1}{\partial\xi_1} + \frac{\partial\phi_1}{\partial x}\frac{\partial\phi_2}{\partial x} + \eta_1\frac{\partial\phi_1}{\partial x}\frac{\partial^2\phi_1}{\partial x\partial z}\right]$$

$$P_3 = -\frac{\partial^2\phi_1}{\partial\tau_1^2} + g\frac{\partial\eta_1}{\partial x}\frac{\partial\phi_1}{\partial\xi_1} - 2\frac{\partial^2\phi_1}{\partial t\partial\tau_2} - 2\frac{\partial^2\phi_2}{\partial t\partial\tau_1} - \frac{\partial\eta_1}{\partial t}\frac{\partial^2\phi_1}{\partial z\partial\tau_1} - \frac{\partial\phi_1}{\partial z}\frac{\partial^2\phi_1}{\partial z\partial\tau_1}$$
$$- \frac{\partial\eta_1}{\partial\tau_1}\frac{\partial^2\phi_1}{\partial z\partial t} - \frac{\partial\eta_2}{\partial t}\frac{\partial^2\phi_1}{\partial z\partial t} - \frac{\partial\phi_2}{\partial z}\frac{\partial^2\phi_1}{\partial z\partial\tau_1} - \frac{\partial\eta_1}{\partial t}\frac{\partial^2\phi_2}{\partial z\partial t} - \frac{\partial\phi_1}{\partial z}\frac{\partial^2\phi_2}{\partial z\partial t} - 2\eta_1\frac{\partial^3\phi_1}{\partial z\partial t\partial\tau_1}$$
$$- 2\eta_2\frac{\partial^3\phi_1}{\partial z\partial t^2} - \eta_1\frac{\partial^3\phi_2}{\partial z\partial t^2} - g\eta_2\frac{\partial^2\phi_1}{\partial z^2} - \frac{\partial\eta_1}{\partial t}\frac{\partial\phi_1}{\partial z}\frac{\partial^2\phi_1}{\partial z^2} - \eta_1\frac{\partial^2\phi_1}{\partial z\partial t}\frac{\partial^2\phi_1}{\partial z^2}$$
$$- g\eta_1\frac{\partial^2\phi_2}{\partial z^2} - \eta_1\frac{\partial\eta_1}{\partial t}\frac{\partial^3\phi_1}{\partial t\partial z^2} - \eta_1\frac{\partial\phi_1}{\partial z}\frac{\partial^3\phi_1}{\partial t\partial z^2} - \frac{1}{2}{\eta_1}^2\frac{\partial^4\phi_1}{\partial z^2\partial t^2} - \frac{1}{2}g{\eta_1}^2\frac{\partial^3\phi_1}{\partial z^3}$$
$$+ g\frac{\partial\eta_1}{\partial\xi_1}\frac{\partial\phi_1}{\partial x} + g\frac{\partial\eta_2}{\partial x}\frac{\partial\phi_1}{\partial x} - \frac{\partial\phi_1}{\partial x}\frac{\partial^2\phi_1}{\partial t\partial\xi_1} + g\frac{\partial\eta_1}{\partial x}\frac{\partial\phi_2}{\partial x} - \frac{\partial\phi_1}{\partial x}\frac{\partial^2\phi_1}{\partial x\partial\tau_1}$$
$$- \frac{\partial\phi_1}{\partial\xi_1}\frac{\partial^2\phi_1}{\partial x\partial t} - \frac{\partial\phi_2}{\partial x}\frac{\partial^2\phi_1}{\partial x\partial t} - \frac{\partial\phi_1}{\partial x}\frac{\partial^2\phi_2}{\partial x\partial t} + g\eta_1\frac{\partial\eta_1}{\partial x}\frac{\partial^2\phi_1}{\partial x\partial z} - \frac{\partial\eta_1}{\partial t}\frac{\partial\phi_1}{\partial x}\frac{\partial^2\phi_1}{\partial x\partial z}$$
$$- \eta_1\frac{\partial^2\phi_1}{\partial x\partial t}\frac{\partial^2\phi_1}{\partial x\partial z} - \eta_1\frac{\partial^2\phi_1}{\partial x\partial t}\frac{\partial^3\phi_1}{\partial x\partial z\partial t}$$

Expressions for $T_{m,n}^{3,\pm}, P_{m,n}^{3,\pm}$ and $Q_{m,n}^{3,\pm}$

$$T_{1,1}^{3,+} = -\frac{g\,\mathrm{sech}\,kh}{2\omega}\left\{2k\cosh k(z+h)\frac{\partial A^+}{\partial\xi_2} + k^2D\sinh k(z+h)\frac{\partial A^-}{\partial\xi_1}\right.$$
$$\left. - i[2k(z+h)\sinh k(z+h) + \cosh k(z+h)]\frac{\partial^2 A^+}{\partial\xi_1^2}\right\}$$

$$T_{1,1}^{3,-} = \frac{g\,\mathrm{sech}\,kh}{2\omega}\left\{2k\cosh k(z+h)\frac{\partial A^-}{\partial\xi_2} + k^2D\sinh k(z+h)\frac{\partial A^+}{\partial\xi_1}\right.$$
$$\left. + i[2k(z+h)\sinh k(z+h) + \cosh k(z+h)]\frac{\partial^2 A^-}{\partial{\xi_1}^2}\right\}$$

$$T_{0,0}^{3,+} = -\frac{\partial^2 B}{\partial \xi_1^2}$$

$$P_{0,0}^{3,+} = \frac{\omega^4 - g^2k^2}{4\omega^2}\frac{\partial\left[A^+\left(A^+\right)^* + A^-\left(A^-\right)^*\right]}{\partial\tau_1} + \frac{g^2k}{2\omega}\frac{\partial\left[A^+\left(A^+\right)^* - A^-\left(A^-\right)^*\right]}{\partial\xi_1} - \frac{\partial^2 B}{\partial\tau_1^2}$$

$$\begin{aligned}P_{1,1}^{3,+} =& g\frac{\partial A^+}{\partial\tau_2} + \frac{ig}{2\omega}\frac{\partial^2 A^+}{\partial\tau_1^2} - \frac{ih\omega^2}{k}\frac{\partial^2 A^+}{\partial\xi_1\partial\tau_1} + \frac{\omega^2 D}{2}\frac{\partial A^-}{\partial\tau_1} - \frac{i\left(\omega^4 + g^2k^2\right)^2}{4g\omega^3}A^+A^-\left(A^-\right)^* \\ &+ \frac{i\left(9g^6k^6 - 12g^4k^4\omega^4 + 13g^2k^2\omega^8 - 2\omega^{12}\right)}{16g\omega^7}\left(A^+\right)^2\left(A^+\right)^* \\ &+ \frac{i\left(\omega^4 - g^2k^2\right)}{2g\omega}A^+\frac{\partial B}{\partial\tau_1} + igkA^+\frac{\partial B}{\partial\xi_1}\end{aligned}$$

$$\begin{aligned}P_{1,1}^{3,-} =& g\frac{\partial A^-}{\partial\tau_2} + \frac{ig}{2\omega}\frac{\partial^2 A^-}{\partial\tau_1^2} + \frac{ih\omega^2}{k}\frac{\partial^2 A^-}{\partial\xi_1\partial\tau_1} + \frac{\omega^2 D}{2}\frac{\partial A^+}{\partial\tau_1} - \frac{i\left(\omega^4 + g^2k^2\right)^2}{4g\omega^3}A^-A^+\left(A^+\right)^* \\ &+ \frac{i\left(9g^6k^6 - 12g^4k^4\omega^4 + 13g^2k^2\omega^8 - 2\omega^{12}\right)}{16g\omega^7}\left(A^-\right)^2\left(A^-\right)^* \\ &+ \frac{i\left(\omega^4 - g^2k^2\right)}{2g\omega}A^-\frac{\partial B}{\partial\tau_1} - igkA^-\frac{\partial B}{\partial\xi_1}\end{aligned}$$

$$Q_{0,0}^{3,+} = 0$$

$$Q_{1,1}^{3,+} = \frac{3iD^2gk^3\,\mathrm{sech}\,kh\left(3gk\cosh 3kh - \omega^2\sinh 3kh\right)}{24gk\omega\sinh 3kh - 8\omega^3\cosh 3kh}A^+$$

$$Q_{1,1}^{3,-} = \frac{3iD^2gk^3\,\mathrm{sech}\,kh\left(3gk\cosh 3kh - \omega^2\sinh 3kh\right)}{24gk\omega\sinh 3kh - 8\omega^3\cosh 3kh}A^-$$

Expressions for coefficients in the ENLS

$$C_g^+ = C_g^- = \frac{\omega}{2k} + h\omega\,\mathrm{csch}\,2kh$$

$$B_1^+ = B_1^- = \frac{i}{2\omega}$$

$$B_2^+ = -B_2^- = -ih\tanh kh$$

$$B_3^+ = B_3^- = -\frac{ih\omega}{2k}\coth kh$$

$$D_1^+ = D_1^- = \frac{D}{2}k\tanh kh$$

$$D_2^+ = -D_2^- = \frac{D}{4}\omega\tanh kh$$

$$D_3^+ = D_3^- = \frac{3iD^2k^2\omega\,\mathrm{csch}\,2kh\left(3gk\cosh 3kh - \omega^2\sinh 3kh\right)}{4\omega^2\cosh 3kh - 12gk\sinh 3kh}$$

$$\sigma_1^+ = \sigma_1^- = \frac{igk^3(20 + 13\cosh 2kh + 2\cosh 4kh + \cosh 6kh)\,\mathrm{csch}^3\,2kh}{8\omega}$$

$$\sigma_2^+ = \sigma_2^- = -\frac{i\left(\omega^4 + g^2k^2\right)^2}{4g^2\omega^3}$$

$$\sigma_3^+ = \sigma_3^- = \frac{i\left(\omega^4 - g^2k^2\right)}{2g^2\omega}$$

$$\sigma_4^+ = -\sigma_4^- = ik$$

$$F_1^+ = F_1^- = \sigma_1^+ - \frac{i\left[2g^2k\omega + C_g^+\left(g^2k^2 - \omega^4\right)\right]^2}{8g^2\omega^3\left[gh - \left(C_g^+\right)^2\right]}$$

$$F_2^+ = F_2^- = \sigma_2^+ - \frac{i\left[-4g^4k^2\omega^2 + \left(\omega^4 - g^2k^2\right)^2\left(C_g^+\right)^2\right]}{8g^2\omega^3\left[gh - \left(C_g^+\right)^2\right]}$$

Expressions for the operators

The first-order operators are defined as

$$\overline{\mathcal{L}}_{\text{flu}}\left[\gamma_{1,1}^{1,\pm}e^{iS_{1,1}^{\pm}}\right] = \mathcal{F}_{1,1}\left(z, -2\frac{\partial^2}{\partial x\partial\xi_1}\gamma_{1,1}^{1,\pm}e^{iS_{1,1}^{\pm}}\right)\cosh k(z+h)$$

where $\mathcal{F}_{1,1}$ is defined in (6.19) and we have

$$\overline{\mathcal{L}}_{\text{bot}}\left[\gamma_{1,1}^{1,-}e^{iS_{1,1}^{-}}\right] = \left[De^{2ikx}\left(-\frac{1}{2}\frac{\partial^2}{\partial z^2} + ik\frac{\partial}{\partial x}\right)\gamma_{1,1}^{1,-}e^{iS_{1,1}^{-}}\Big|_{z=-h}\right]\frac{\sinh k(z+h)}{k}$$

$$\overline{\mathcal{L}}_{\text{bot}}\left[\gamma_{1,1}^{1,+}e^{iS_{1,1}^{+}}\right] = \overline{\mathcal{L}}_{\text{bot}}^{(1)}\left[\gamma_{1,1}^{1,+}e^{iS_{1,1}^{+}}\right] + \overline{\mathcal{L}}_{\text{bot}}^{(2)}\left[\gamma_{1,1}^{1,+}e^{iS_{1,1}^{+}}\right]$$

and

$$\overline{\mathcal{L}}_{\text{bot}}^{(1)}\left[\gamma_{1,1}^{1,+}e^{iS_{1,1}^{+}}\right] = \left[De^{-2ikx}\left(-\frac{1}{2}\frac{\partial^2}{\partial z^2} - ik\frac{\partial}{\partial x}\right)\gamma_{1,1}^{1,+}e^{iS_{1,1}^{+}}\Big|_{z=-h}\right]\frac{\sinh k(z+h)}{k}$$

$$\overline{\mathcal{L}}_{\text{bot}}^{(2)}\left[\gamma_{1,1}^{1,+}e^{iS_{1,1}^{+}}\right] = \left[De^{2ikx}\left(-\frac{1}{2}\frac{\partial^2}{\partial z^2} + ik\frac{\partial}{\partial x}\right)\gamma_{1,1}^{1,+}e^{iS_{1,1}^{+}}\Big|_{z=-h}\right]\left\{\frac{\sinh 3k(z+h)}{3k} + \frac{\omega^2\tanh 3kh - 3gk}{9gk^2\tanh 3kh - 3k\omega^2}\cosh 3k(z+h)\right\}$$

in which, the superscripts (1) and (2) are for modes $e^{iS_{1,1}^{+}}$ and $e^{iS_{3,1}^{+}}$, respectively. For the second-order operators, we have

$$\mathcal{L}_{\text{flu}}\left[\phi_1,\phi_2\right] = -\int_{-h}^{0}\left(-\frac{\partial^2\phi_1}{\partial\xi_1^2} - 2\frac{\partial^2\phi_2}{\partial x\partial\xi_1}\right)\psi^+dz$$

$$\mathcal{L}_{\text{sur}}\left[\phi_1,\phi_2\right] = \left(-\frac{\partial^2\phi_1}{\partial\tau_1^2} - 2\frac{\partial^2\phi_2}{\partial t\partial\tau_1}\right)\frac{\psi^+}{g}\Big|_{z=0}$$

$$\mathcal{L}_{\text{bot}}\left[\phi_1,\phi_2\right] = \zeta\left\{-\left[-\frac{\partial\sigma}{\partial x}\frac{\partial\phi_1}{\partial\xi_1} + \left(\frac{\partial\sigma}{\partial x}\frac{\partial}{\partial x} - \sigma\frac{\partial^2}{\partial z^2}\right)\phi_2\right]\psi^+\Big|_{z=-h}\right\}$$

which are bilinear operators on ϕ_1, the component at $O(\varepsilon)$, and ϕ_2, at $O\left(\varepsilon^2\right)$. And ζ is the operator to take out the term of mode $e^{iS_{1,1}^{+}}$.

6.3. *Appendix C. Derivation for the solution of the linearized equations*

In this subsection, we present the details of the exact solution for the BVP in subsection 3.1. The linear differential system can be expressed in matrix form,

$$U'(x) = \mathcal{A}^{-1}\mathcal{B}\mathcal{U}(x) \tag{6.29}$$

in which $\mathcal{U}(x)$ is a column vector, $\mathcal{A}$ and $\mathcal{B}$ are matrix, with $\mathcal{A}^{-1}$ being the inverse matrix of $\mathcal{A}$, giving by

$$\begin{gathered}\mathcal{U}(x) = (R(x), T(x))^{\mathrm{T}} \\ \mathcal{A} = \begin{pmatrix} S_3^+ & S_4^+ \\ S_4^- & S_3^- \end{pmatrix}, \mathcal{B} = \begin{pmatrix} S_1^+ & S_2^+ \\ S_2^- & S_1^- \end{pmatrix}\end{gathered} \tag{6.30}$$

Let's imply a linear transform to $\mathcal{U}(x)$,

$$\mathcal{V}(x) = Q\mathcal{U}(x) \tag{6.31}$$

where $\mathcal{V}(x)$ is a column vector with two components $\tilde{R}(x)$ and $\tilde{T}(x)$, and Q is a constant matrix, defined as follows.

$$\begin{gathered}\mathcal{V}(x) = (\tilde{R}(x), \tilde{T}(x))^{\mathrm{T}} \\ Q = \begin{pmatrix} -Q_2 - P\,\mathrm{sgn}\left(P^2\right) & -Q_2 + P\,\mathrm{sgn}\left(P^2\right) \\ Q_1 & Q_1 \end{pmatrix}\end{gathered} \tag{6.32}$$

in which Q_1 and Q_2 are real parameters, defined as

$$Q_1 = i\frac{S_1^+S_4^+ + S_2^+S_3^+}{\left(S_4^+\right)^2 - \left(S_3^+\right)^2} \tag{6.33}$$

and

$$Q_2 = i\frac{S_1^+S_3^+ + S_2^+S_4^+}{\left(S_4^+\right)^2 - \left(S_3^+\right)^2} \tag{6.34}$$

And P is a complex, given by

$$P = \sqrt{\frac{\left(S_1^+\right)^2 - \left(S_2^+\right)^2}{\left(S_4^+\right)^2 - \left(S_3^+\right)^2}} \tag{6.35}$$

Let us denote the sign function of P^2 as $\mathrm{sgn}\left(P^2\right)$, which is equal to 1 for $P^2 > 0$ and to -1 for $P^2 < 0$. Under the linear transform, (6.29) is converted into

$$\mathcal{V}'(x) = C\mathcal{V}(x) \tag{6.36}$$

where $C = Q\mathcal{A}^{-1}\mathcal{B}Q^{-1}$, being a diagonal matrix:

$$C = \begin{pmatrix} iP & 0 \\ 0 & -iP \end{pmatrix} \tag{6.37}$$

Since $\left(S_4^+\right)^2 - \left(S_3^+\right)^2 > 0$, the sign of $\left(S_1^+\right)^2 - \left(S_2^+\right)^2$ is the same as P^2, which results in $\mathrm{sgn}\left(\left(S_1^+\right)^2 - \left(S_2^+\right)^2\right) = \mathrm{sgn}\left(P^2\right)$. Thus, we discuss the solutions in terms of $P^2 > 0, < 0$ and $= 0$, respectively. For $P^2 \neq 0$ The uncoupled linear system is easily solvable with general solution, expressed as

$$v(x) = \left(C_1 e^{iPx}, C_2 e^{-iPx}\right)^{\mathrm{T}} \tag{6.38}$$

The general solution of $U(x)$ can be secured by utilizing the inverse transformation of (6.31). This, in conjunction with the conditions specified in (3.5) and (3.11), yields the value for C_1

and C_2. Following this, the solutions for $R(x)$ and $T(x)$ can be ascertained.

$$\begin{aligned} R(x) &= \frac{-Q_1 \sin P(L-x)}{iP\,\mathrm{sgn}\left(P^2\right)\cos PL + Q_2 \sin PL} \\ T(x) &= \frac{iP\,\mathrm{sgn}\left(P^2\right)\cos P(L-x) + Q_2 \sin P(L-x)}{iP\,\mathrm{sgn}\left(P^2\right)\cos PL + Q_2 \sin PL} \end{aligned} \tag{6.39}$$

For $P^2 > 0$

$$\begin{aligned} R(x) &= \frac{-iQ_1 \sinh P_b(L-x)}{iP_b \cosh P_b L - Q_2 \sinh P_b L} \\ T(x) &= \frac{iP_b \cosh P_b(L-x) - Q_2 \sinh P_b(L-x)}{iP_b \cosh P_b L - Q_2 \sinh P_b L} \end{aligned} \tag{6.40}$$

For $P^2 < 0$

P is a pure imaginary number. By introducing a real parameter, $P_b = iP$, the solutions are

$$\begin{aligned} R(x) &= \frac{-iQ_1 \sinh P_b(L-x)}{iP_b \cosh P_b L - Q_2 \sinh P_b L} \\ T(x) &= \frac{iP_b \cosh P_b(L-x) - Q_2 \sinh P_b(L-x)}{iP_b \cosh P_b L - Q_2 \sinh P_b L} \end{aligned} \tag{6.41}$$

For $P^2 = 0$

We take $P \to 0$ in (6.40) to obtain

$$\begin{aligned} R(x) &= \frac{-Q_1(L-x)}{i + Q_2 L} \\ T(x) &= \frac{i + Q_2(L-x)}{i + Q_2 L} \end{aligned} \tag{6.42}$$

In summary, regardless of the value of P, reflectance $\tilde{R}$ and transmittance $\tilde{T}$ can be expressed as follows.

$$\begin{aligned} \tilde{R} &= |R(0)| = \sqrt{\frac{Q_1^2}{|P\cot PL|^2 + Q_2^2}} \\ \tilde{T} &= |T(L)| = \sqrt{\frac{|P|^2}{|P\cot PL|^2 + Q_2^2|\sin PL|^2}} \end{aligned} \tag{6.43}$$

6.4. *Appendix D. Magnitude of the downshift of the wave frequency*

Assuming that the magnitude of the frequency shift δ is small, i.e., $\delta \ll O(1)$, we can demonstrate that $P^2 < 0$, resulting in the substitution of $|P\cot PL|$ with $iP_b \cosh P_b L$, with $P_b = iP$, as detailed in Appendix 6.3. Combining (3.20) with (3.16) then provides an implicit relation for δ as follows.

$$\Gamma(\omega', D)|_{\omega'=\delta} = 0 \tag{6.44}$$

in which $\Gamma(\omega', D)$ is a binary function on ω' and D, defined as

$$\Gamma(\omega', D) = 2\left\{Q_2^2 + (iP_b \cosh P_b L)^2\right\}\frac{\partial Q_1}{\partial \omega'} - Q_1\left\{\frac{\partial Q_2^2}{\partial \omega'} + \frac{\partial\,(iP_b \cosh P_b L)^2}{\partial \omega'}\right\} \tag{6.45}$$

Applying the first-order Taylor expansion to Γ in terms of ω' results in

$$\Gamma(\delta, D) = \Gamma(0, D) + \frac{\partial \Gamma(0, D)}{\partial \omega'}\delta + O\left(\delta^2\right) = 0 \tag{6.46}$$

which leads to an approximate explicit solution for δ by eliminating the high-order error,

$$\delta = \Lambda(D) + O(\delta) \approx \Lambda(D) \tag{6.47}$$

in which $\Lambda(D)$ is a function relying on D :

$$\Lambda(D) = \left(\frac{\partial \log|\Gamma(0, D)|}{\partial \omega'}\right)^{-1} \tag{6.48}$$

It is necessary to further simplify the highly intricate expression of $\Lambda(D)$. This can be done through the application of a second-order Taylor expansion, as expressed below:

$$\Lambda(D) \approx \delta_0 + \delta_1 D + \delta_2 D^2 + O\left(D^3\right) \tag{6.49}$$

where $\delta_1 = d\Lambda(0)/dD = 0$. Let δ_0 and $2\delta_2$ represent $\Lambda(0)$ and $d^2\Lambda(0)/dD^2$, respectively. We have

$$\delta_0 = \frac{3iC_g^+\left(E_3 + iE_1C_g^+\right)}{6E_2E_3C_g^+ - iL^2D_0^+} \tag{6.50}$$

and

$$\delta_2 = \frac{\eth_4 L^4 + \eth_2 L^2}{5C_g^+\left(6E_2E_3C_g^+ - iL^2D_0^+\right)^2} \tag{6.51}$$

in which

$$\eth_4 = E_3D_0^{+3} + iC_g^+D_0^{+2}\left(5D_3^+ + 6E_1D_0^+\right) \tag{6.52}$$

and

$$\begin{aligned}\eth_2 = 15\{&-E_3^3D_0^+ - 2iE_1E_3^2C_g^+D_0^+ + iE_1C_g^{+3}D_3^+\left(E_1 + 2E_2D_0^+\right)\\ &+E_1E_3C_g^{+2}\left[D_3^+ + D_0^+\left(E_1 - 2E_2D_0^+\right)\right]\}\end{aligned} \tag{6.53}$$

Thus, an approximate solution for the frequency downshift of the Bragg resonance is expressed as

$$\delta = \frac{3iC_g^+\left(E_3 + iE_1C_g^+\right)}{6E_2E_3C_g^+ - iL^2D_0^+} + \frac{\eth_4 L^4 + \eth_2 L^2}{5C_g^+\left(6E_2E_3C_g^+ - iL^2D_0^+\right)^2} \tag{6.54}$$

REFERENCES

Akhmediev, N., Ankiewicz, A. and Taki, M., 2009 Waves that appear from nowhere and disappear without a trace, *Phys. Lett. A*, **373 (6)**, pp. 675-678.

Ardhuin, F. and Herbers, T. 2002 Bragg scattering of random surface gravity waves by irregular seabed topography, *J. Fluid Mech.*, **451**, pp. 1-33.

Ardhuin, F. and Magne, R. 2007 Scattering of surface gravity waves by bottom topography with a current, *J. Fluid Mech.*, **576**, pp. 235-264.

Benjamin, T. B. and Feir, J. E. 1967 The reflection of wave energy by undulations on the seabed, *J. Fluid Mech.*, **27(3)**, pp. 417-430.

Davies, A.G. and Heathershaw, A.D. 1984 Surface-wave propagation over sinusoidally varying topography, *J. Fluid Mech.*, **144**, pp. 419-443.

Fan, J., Zheng, J., Tao, A. and Liu, Y. 2021 Upstream-propagating waves induced by steady current over a rippled bottom: Theory and experimental observation, *J. Fluid Mech.*, **910**, pp. A49.

Fang, H., Tang, L. and Lin, P. 2023 Homotopy analysis of wave transformation over permeable seabeds and porous structures, *Ocean Eng.*, **274**, pp. 114087.

Gao, J., Ma, X., Dong, G., Chen, H., Liu, Q. and Zang, J. 2021 Investigation on the effects of bragg reflection on harbor oscillations, *Coast. Eng.*, **170**, pp. 103977.

Guazzelli, E., Rey, V. and Belzons, M. 1992 Higher-order Bragg reflection of gravity surface waves by periodic beds, *J. Fluid Mech.*, **245**, pp. 301-317.

Hammack, J.L., Henderson, D.M. and Segur, H. 2005 Progressive waves with persistent two-dimensional surface patterns in deep water, *J. Fluid Mech.*, **532**, pp. 1-52.

Hara, T. and Mei, C.C. 1988 Bragg scattering of surface waves by periodic bars: theory and experiment, *J. Fluid Mech.*, **106**, pp. 22575-22592.

Howard, L.N. and Yu, J. 2007 Normal modes of a rectangular tank with corrugated bottom, *J. Fluid Mech.*, **593**, pp. 209-234.

Kirby, J.T. 1998 Current effects on resonant reflection of surface water waves by sand bars, *J. Fluid Mech.*, **186**, pp. 501-520.

Kirby, J.T. 1993 A note on bragg scattering of surface waves by sinusoidal bars, *Physics of Fluids A: Fluid dynamics*, **5 (2)**, pp. 380-386.

Laffitte, E., Rey, V., Touboul, J. and Belibassakis, K. 2021 Water wave scattering by a sinusoidal bed in the presence of vertically sheared current, *Appl. Ocean Res.*, **108**, pp. 102549.

Lake, B.M., Yuen, H.C., Rungaldier, H. and Ferguson, W.E. 1977 Nonlinear deep-water waves: Theory and experiment. Part 2. Evolution of a continuous wave train, *J. Fluid Mech.*, **83 (1)**, pp. 49-74.

Liang, B., Ge, H., Zhang, L. and Liu, Y. 2020 Wave resonant scattering mechanism of sinusoidal seabed elucidated by mathieu instability theorem, *Ocean Eng.*, **218**, pp. 108238.

Liao, B., Dong, G., Ma, Y. and Gao, J.L. 2017 Linear-shear-current modified schrdinger equation for gravity waves in finite water depth, *Phys. Rev. E*, **96 (4)**, pp. 043111.

Liu, H.-W., Luo, H. and Zeng, H.-D. 2015 Optimal collocation of three kinds of bragg breakwaters for bragg resonant reflection by long waves, *J. Waterw. Port Coast.*, **14 (3)**, pp. 04014039.

Liu, H.W., Li, X.F. and Lin, P.Z. 2019 Analytical study of bragg resonance by singly periodic sinusoidal ripples based on the modified mild-slope equation, *Coast. Eng.*, **150**, pp.121-134.

Liu, H.W. and Zhou, X.M. 2014 Explicit modified mild-slope equation for wave scattering by piecewise monotonic and piecewise smooth bathymetries, *J. Fluid Mech.*, **87 (1)**, pp. 29-45.

Liu, Y. and Yue, D.K.P. 1998 On generalized bragg scattering of surface waves by bottom ripples, *J. Fluid Mech.*, **356**, pp. 297-326.

Madsen, P.A., Fuhrman, D.R. and Wang, B. 2005 A boussinesq-type method for fully nonlinear waves interacting with a rapidly varying bathymetry, *Coast. Eng.*, **53 (5-6)**, pp.487-504.

Magne, R., Rey, V. and Ardhuin, F. 2005 Measurement of wave scattering by topography in the presence of currents, *Phys. Fluids*, **17 (12)**, pp.126601.

Mei, C.C. 2005 Resonant reflection of surface water waves by periodic sandbars, *J. Fluid Mech.*, **152**, pp.315-335.

Mei, C.C., Hara, T. and Naciri, M. 2005 Note on bragg scattering of water waves by parallel bars on the seabed, *J. Fluid Mech.*, **186**, pp.147-162.

Onorato, M., Osborne, A.R. and Serio, M. 2006 Modulational instability in crossing sea states: A possible mechanism for the formation of freak waves, *Phys. Rev. Lett.*, **96 (1)**, pp. 014503.

Peng, J., Tao, A , Liu, Y., Zheng, J., Zhang, J. and Wang, R. 2019 A laboratory study of class III Bragg resonance of gravity surface waves by periodic beds, *Phys. Fluids*, **31**, pp. 067110.

Rey, V., Guazzelli, É. and Mei, C.C. 1996 Resonant reflection of surface gravity waves by one-dimensional doubly sinusoidal beds, *Phys. Fluids*, **8 (6)**, pp. 1525-1530.

Thomas, R., Kharif, C. and Manna, M. 2012 A nonlinear schrödinger equation for water waves on finite depth with constant vorticity, *Phys. Fluids*, **24 (12)**, pp. 127102.

Yu, J. and Howard, L.N. 2012 Exact floquet theory for waves over arbitrary periodic topographies, *J. Fluid Mech.*, **712**, pp. 451-470.